Bio-Design and Manufacturing (2024) 7:517–547
https://doi.org/10.1007/s42242-024-00300-7

REVIEW

Recent developments in selective laser processes for wearable devices

Youngchan Kim[1] · Eunseung Hwang[1] · Chang Kai[2] · Kaichen Xu[3] · Heng Pan[2] · Sukjoon Hong[1]

Received: 27 November 2023 / Accepted: 2 June 2024 / Published online: 22 July 2024

Abstract

Recently, the increasing interest in wearable technology for personal healthcare and smart virtual/augmented reality applications has led to the development of facile fabrication methods. Lasers have long been used to develop original solutions to such challenging technological problems due to their remote, sterile, rapid, and site-selective processing of materials. In this review, recent developments in relevant laser processes are summarized under two separate categories. First, transformative approaches, such as for laser-induced graphene, are introduced. In addition to design optimization and the alteration of a native substrate, the latest advances under a transformative approach now enable more complex material compositions and multilayer device configurations through the simultaneous transformation of heterogeneous precursors, or the sequential addition of functional layers coupled with other electronic elements. In addition, the more conventional laser techniques, such as ablation, sintering, and synthesis, can still be used to enhance the functionality of an entire system through the expansion of applicable materials and the adoption of new mechanisms. Later, various wearable device components developed through the corresponding laser processes are discussed, with an emphasis on chemical/physical sensors and energy devices. In addition, special attention is given to applications that use multiple laser sources or processes, which lay the foundation for the all-laser fabrication of wearable devices.

Youngchan Kim and Eunseung Hwang have contributed equally to this work.

✉ Heng Pan
hpan@tamu.edu

✉ Sukjoon Hong
sukjoonhong@hanyang.ac.kr

[1] Optical Nanoprocessing Lab, Department of Mechanical Engineering, BK21 FOUR ERICA-ACE Center, Hanyang University, 55 Hanyangdaehak-Ro, Sangnok-Gu, Ansan 15588, Republic of Korea

[2] Multiscale Manufacturing Lab, J. Mike Walker '66 Department of Mechanical Engineering, Texas A&M University, College Station, TX 77843, USA

[3] State Key Laboratory of Fluid Power and Mechatronic Systems, School of Mechanical Engineering, Zhejiang University, Hangzhou 310058, China

Graphic abstract

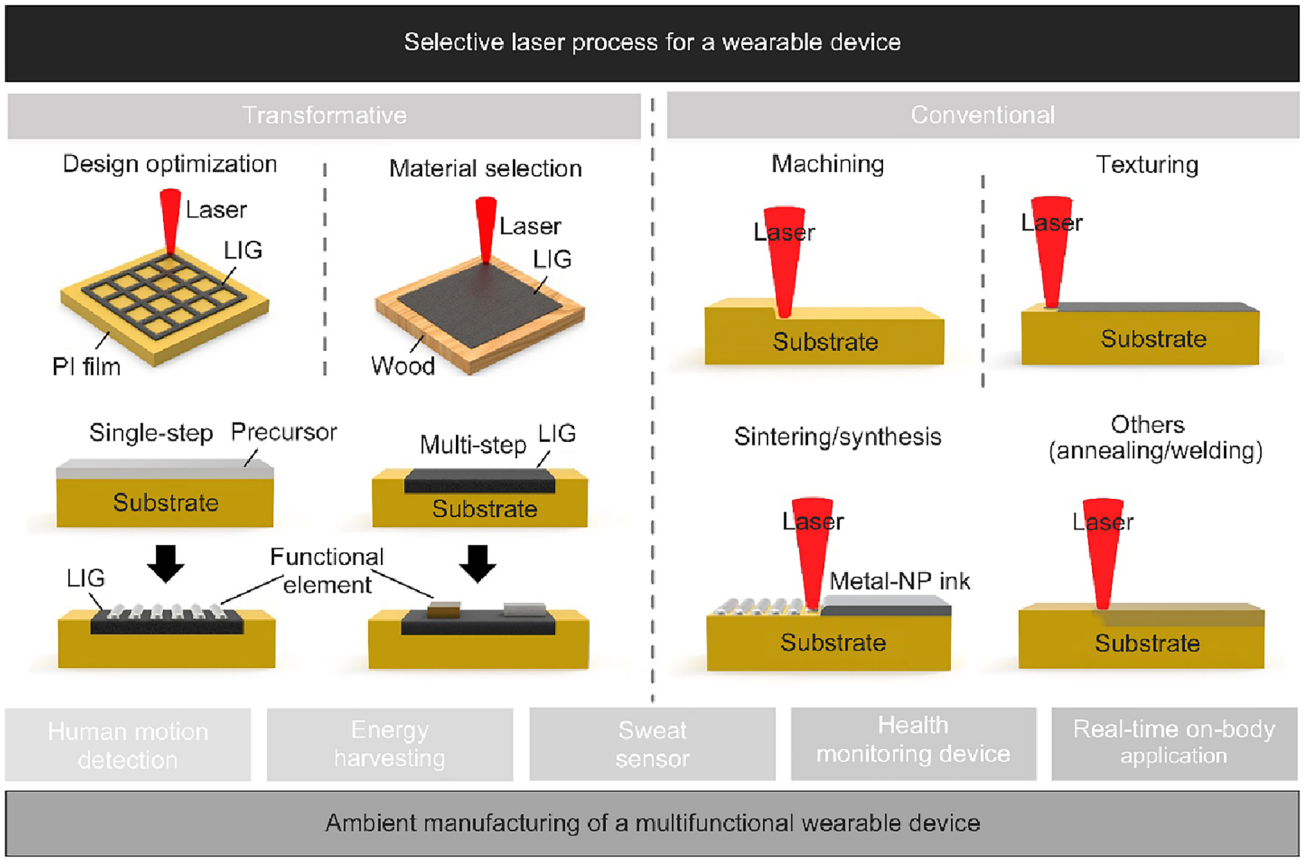

Keywords Selective laser process · Wearable device · Transformative approach · Laser-induced graphene · Ablation · Sintering · Synthesis

Introduction

The emergence of wearable devices can be attributed to several key factors and global trends. Rapid advances in microelectronics have enabled the creation of smaller, faster, and more energy-efficient components that can be integrated into a single device. Moreover, the demand for portable devices and new forms of electronics has fostered the fabrication of electronics on flexible or stretchable substrates. From the perspective of consumer demand, interest in health monitoring has been increasing. This trend suggests that this interest will continue in the future, as the percentage of elderly people who require intensive and prolonged health care is rapidly increasing in many countries. The outbreak of the COVID-19 pandemic has also had a significant impact on the interest in and adoption of wearable devices [1]. These factors, as well as virtual reality (VR) and augmented reality, have contributed to the emergence and proliferation of wearable devices in various sectors, from consumer electronics to health care. Therefore, the wearable technology industry is expected to continue to evolve with ongoing innovations and developments in response to changing consumer requirements and technological capabilities.

The fabrication of technologies developed for conventional electronics and new types of electronics, such as flexible, stretchable, and wearable devices, poses several problems and limitations. The most glaring problem is that conventional electronics often involve high-temperature processes that cannot be used with the heat-sensitive flexible substrates in wearable electronics [2]. These substrates may deform, melt, or degrade at elevated temperatures, which makes the application of traditional techniques challenging. Functional materials [3] and novel structural designs [4] for wearable devices have been keenly investigated. Conventional fabrication technologies are often not fully compatible with new materials, such as low-dimensional nanomaterials, and the frequent design changes that are inevitable at

the early developmental stage also impose a burden on conventional photolithography-based fabrication methods. To address these challenges, researchers and engineers have been developing new fabrication techniques that are tailored to the specific requirements of wearable electronics. We expect that the selective laser process will significantly contribute to this.

Lasers are highly sought tools for material processing because of their unique properties, such as monochromaticity, high-energy density, and tunability. The laser process is fundamentally a selective operation because it only affects the areas irradiated by the laser. The laser-based control of light sources enables the precise irradiation of a target area. The ability to focus on a spot that is sized between a few micrometers and several nanometers facilitates precision machining [5]. This high-precision processing capability facilitates complex designs and three-dimensional (3D) processing [6], and it allows for the processing of various materials through the choice of wavelengths based on the optical properties of the target material [7]. Alternatively, the selection of temporal pulse modulation can be achieved using lasers ranging from continuous-wave (CW) pulses to ultrashort pulses in the femtosecond regime [8]. Based on this, selective laser processing can fabricate highly customized devices through precise control of spatiotemporal responses.

Thus, laser-based material processing has been extensively researched [9], whereas selective laser processing has recently been adopted for the prototyping of wearable devices at the laboratory scale [10, 11]. Therefore, we provide a timely summary of the current advances in selective laser processes for wearable devices and discuss future directions in development. In this review, the research on selective laser processing for wearable devices is divided into two categories—transformative and conventional—as shown in Fig. 1. Since the discovery of laser-induced graphene (LIG) in 2014 [12], the number of publications related to the transformative approach has rapidly increased. Consequently, the transformative approach has become an indispensable laser process for wearable devices; in-depth research into this approach not only increases the types of applicable materials but also establishes new methods for creating more complex multilayer devices. Furthermore, conventional laser processes, such as micromachining, ablation, texturing, sintering, synthesis, and annealing, for use in the fabrication of wearable devices have been constantly evolving in tandem with transformative approaches. For a more timely review of the latest studies, we mainly focus on studies published within the recent five years. Any research that involved a vacuum environment was excluded.

Transformative laser process

The main difference between the aforementioned transformative approach and the conventional approach is mainly whether the material is transformed or not. Conventional laser processes such as laser texturing, ablation, and sintering mainly focus on surface treatment, material removal, or material adhesion. They do not result in conversion to a new material, even though minor changes in the material may occur. In contrast, the transformation process completely transforms the original material into a new material; for example, a polyimide (PI) film is transformed into LIG with completely different properties. These transformations selectively impart properties to existing materials, thereby enabling their functional application. This transformative approach makes it easy to create flexible and biocompatible electronic devices and can be used in the development of wearable devices through the design optimization or conversion of various materials. This section discusses how this transformative approach can be used in various wearable devices.

Design optimization

LIG has attracted significant interest in the field of wearable devices because of its excellent mechanical properties, electrical conductivity, 3D porous structure, and cost-effectiveness. LIG is easily produced via thermal decomposition and carbonization by subjecting a polymer material to laser irradiation to induce a photothermal reaction [12]. Notably, LIG that is generated by a laser exhibits a variety of shapes and chemical/physical properties, depending on the laser processing parameters, including laser power [12], working distance [13], hatch size, and spot size [14]. This is because the photothermal reaction is affected by modulating the energy density delivered by the laser, which depends on the laser parameters. The characteristics of LIG, which vary depending on the laser processing conditions, enable multiple functions in wearable devices. For example, recent research has led to the development of a triboelectric nanogenerator (TENG) and a touch sensor using long-fiber LIG (LF-LIG), which was achieved by controlling the working distance of the laser [13] (Fig. 2a). LF-LIG demonstrates excellent triboelectric properties owing to its larger surface area and better energy generation functionality than conventional LIG. Triboelectric properties enable the harvesting of energy by attaching a device to the skin and harvesting electricity through simple contact. As shown in Fig. 2b, an arc-structured LIG shape can be obtained under high-temperature and low-pressure conditions using a millimeter-sized laser spot, and a wave-like array LIG is created by adjusting the hatch size. This structure is sensitive to deformation due to stress concentration along a large

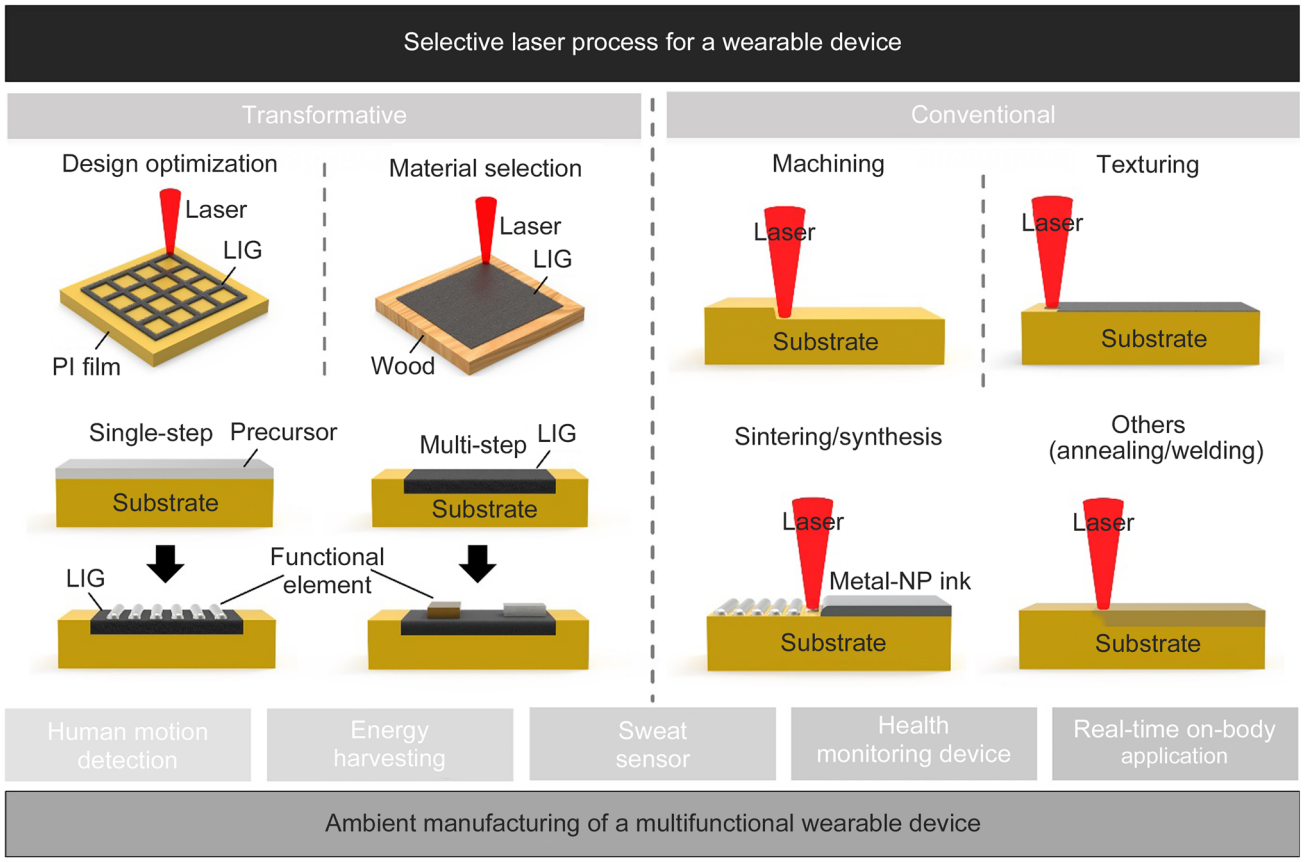

Fig. 1 Overall classification of selective laser processes for wearable devices: transformative and conventional laser processing. The proposed fabrication methods result in multifunctional wearable devices that can be used for human motion detection, energy harvesting, sweat diagnostics, health monitoring, and real-time on-body operation

radius of curvature. Based on these properties of LIG, a foot pad sensor was developed to monitor the user's health status using a piezoresistive sensor [14].

The properties of LIG can be enhanced by adjusting laser parameters or through structural laser patterning in one, two, or three dimensions. Various functional sensors can be fabricated through the use of patterned LIG. Selective laser processing enables precise fabrication and complex design patterning, thereby improving the entire device performance through design optimization [15]. For example, as shown in Fig. 2c, an LIG-based strain sensor fabricated under the same laser processing conditions indicates that a sensor with mesh patterns has better sensitivity to resistance changes due to mechanical strain when compared to a sensor without patterns [16]. In mesh pattern sensors, when the pattern width is reduced, cracks are likely to form inside the LIG, which causes the resistance to change dramatically. Such ultrahigh-sensitivity strain sensors can detect even fine pulses in the wrist and can be effectively applied to skin-attached sensors that track real-time signals. Moreover, the use of complex patterns, such as circles, can make LIG a resistance-enhanced, flexible temperature sensor that offers low-power consumption and stable performance [17] (Fig. 2d). In addition, the patterning process can be applied not only to two-dimensional (2D) patterning but also to 3D shapes [18], including one-dimensional (1D) fibers that are difficult to process [19, 20]. One-dimensional LIG fibers can be assembled in many ways, such as in 2D nanosheets or plates by taking advantage of their flexibility and thin diameters, while retaining excellent flexibility, rigidity, and lightness, unlike nanosheets having different dimensions. These 1D LIG fibers can be used as multifunctional sensors for various applications, including the detection of liquid and the monitoring of airflow and respiration [20] (Fig. 2e).

In addition to the laser process parameters, the environmental atmosphere can affect the properties of LIG. In contrast to other process technologies, the laser process does not require a specific environmental atmosphere because of the rapid response of the laser [21]. However, it is also true that different results can be obtained during the preparation of LIG by changing the environmental atmosphere. In the

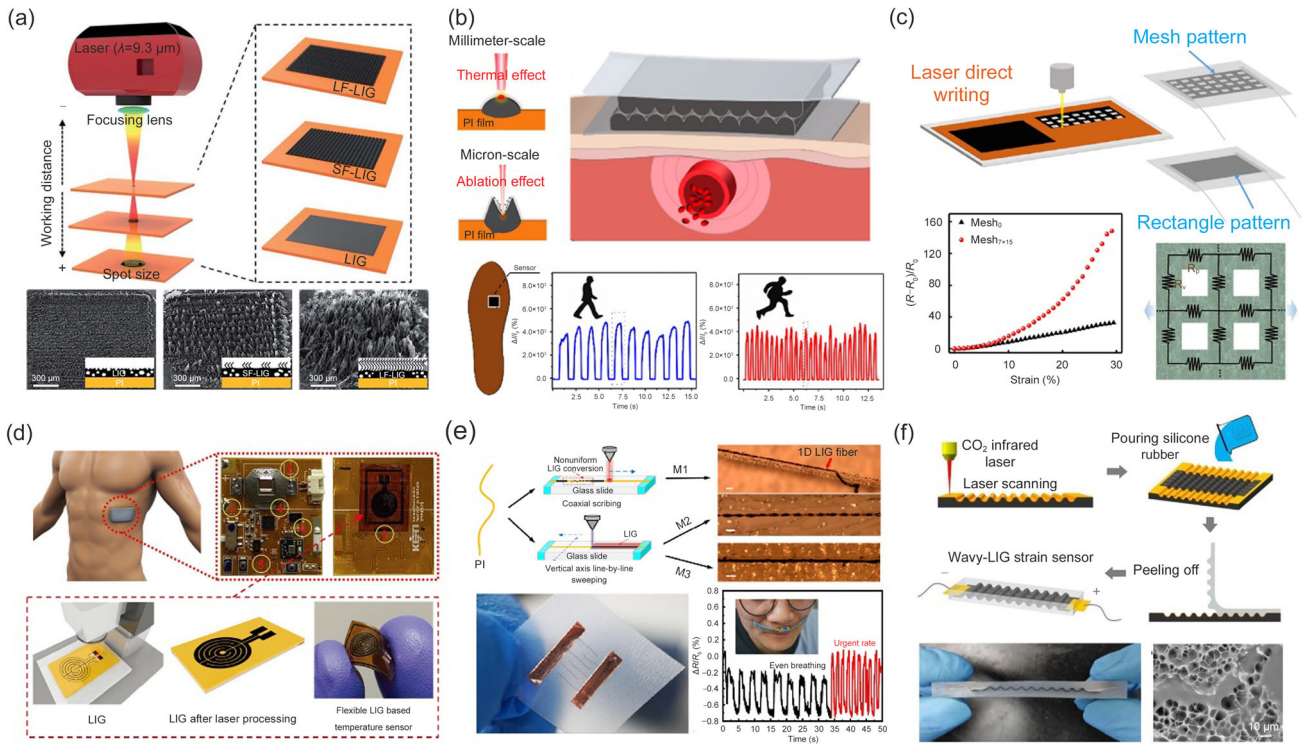

Fig. 2 **a** Schematic illustration of the change in laser-induced graphene (LIG) shape according to the adjustment in working distance. Scanning electron microscopy (SEM) images of three different forms of LIG. Reproduced from Ref. [13], Copyright 2020, with permission from The Royal Society of Chemistry. **b** Schematic of the morphologies of LIG depending on laser spot size (top left); schematic illustration of a wave-shaped array LIG-based pressure sensor (top right); graphs of power change in pressure sensor according to human movement (bottom). Reproduced from Ref. [14], Copyright 2022, with permission from Elsevier. **c** Graph of relative change in resistance of the strain sensor through LIG mesh patterning. Reproduced from Ref. [16], Copyright 2020, with permission from the American Chemical Society. **d** Process schematic of a circularly patterned LIG-based temperature detection sensor. Reproduced from Ref. [17], Copyright 2020, with permission from WILEY–VCH Verlag GmbH & Co. KGaA, Weinheim. **e** Process schematic of 1D LIG fiber (top): an image of LIG-enabled fiber electronics wire (bottom left); graph of respiratory monitoring performance (bottom right). Reproduced from Ref. [20], Copyright 2020, with permission from Elsevier. **f** Process schematic of a wavy-LIG strain sensor (top); a sample of a wavy-LIG strain sensor (bottom left): an SEM image of LIG filled with silicon (bottom right). Reproduced from Ref. [18], Copyright 2020, with permission from the authors, licensed under CC BY 4.0

work done by Li et al. [22], the properties of LIG, particularly wettability, were tuned by changing the gas atmosphere. The contact angle changed from 0° (superhydrophilic) in an O_2 or air atmosphere to >150° (superhydrophobic) in Ar, H_2, or SF_6. The reason behind the difference was estimated to be the dissimilar surface morphology and chemical composition of the LIG prepared in an altered type of gas atmosphere. It was further proved that the performance of the LIG-based application, in this case, the microsupercapacitor, was significantly affected by the detailed LIG preparation techniques. In this regard, we predict that the examination and optimization of other environmental conditions, including the gas atmosphere, according to each application will become an important topic for LIG.

In addition to its aforementioned tunability, LIG can be converted to other materials and used to develop devices having new functionalities. The 3D porous structure of LIG enables converting it to an elastomer substrate while maintaining its shape through the complete penetration of the liquid elastomer [18] (Fig. 2f). Thus, the LIG transferred not only maintains its mechanical properties but also gains flexibility and elasticity; thus, it can be used under high deformation. Its 3D porous structure makes it flexible and allows it to be shaped in different ways, which is beneficial for wearable devices [23] and skin-attached sensors [24, 25] that require elasticity.

Different native materials

In addition to PI films [26], other crosslinked synthetic organic materials, such as colorless polyimide (cPI) [27], polyamide-imide (PAI), and polyetherimide (PEI), can undergo transformative laser processes for the fabrication of graphene [28]. In addition to above-mentioned polymer

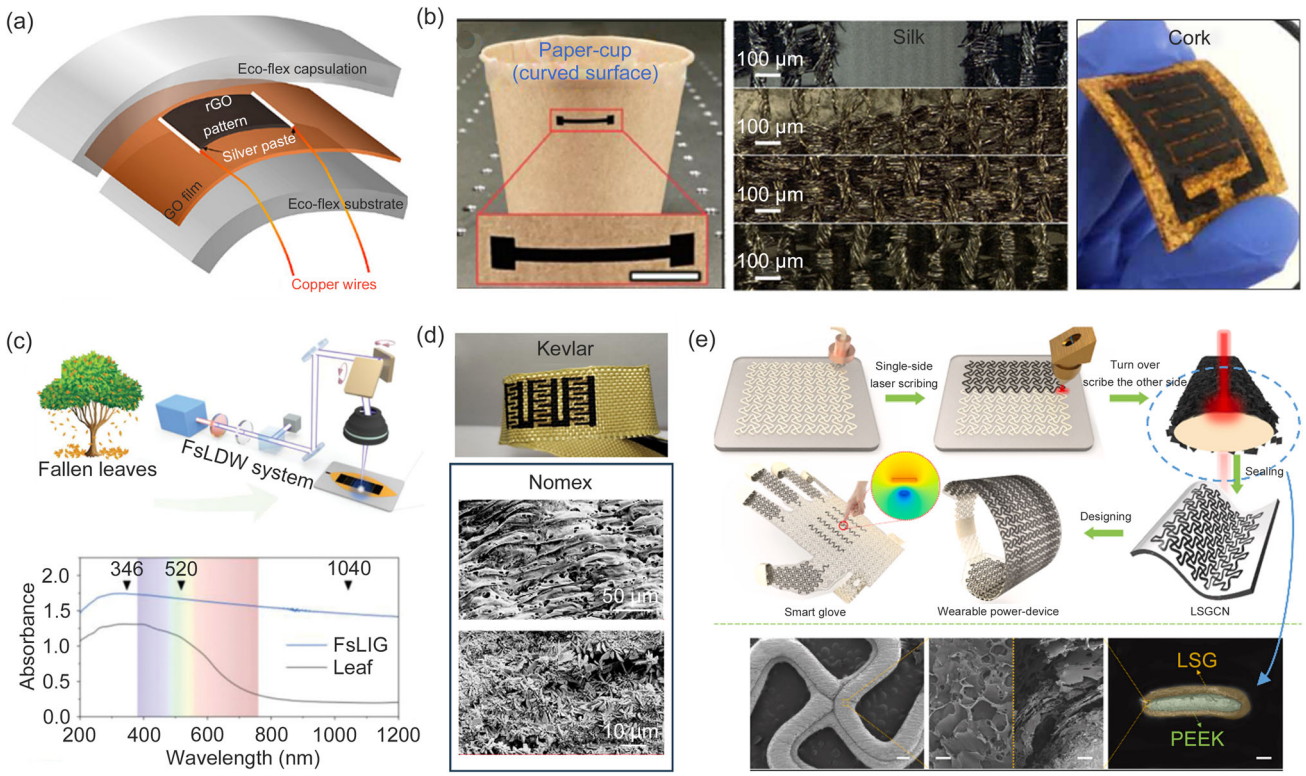

Fig. 3 **a** Schematic layout of the laser-scribed graphene (LSG)-based single sensor. Reproduced from Ref. [33], Copyright 2020, with permission from the American Chemical Society. **b** Left: an image of laser-induced graphene (LIG) pattern on paper (reproduced from Ref. [38], Copyright 2022, with permission from Elsevier); middle: images of LIG pattern on silk (reproduced from Ref. [42], Copyright 2021, with permission from Wiley–VCH GmbH); right: an image of LIG pattern on cork (reproduced Ref. [39], Copyright 2022, with permission from the authors, licensed under CC BY 4.0). **c** Process schematic illustration of the production of LIG with leaves (top); light absorption spectrum of a leaf (bottom). Reproduced from Ref. [43], Copyright 2021, with permission from Wiley–VCH GmbH. **d** Top: an image of LIG pattern on Kevlar (reproduced from Ref. [53], Copyright 2022, with permission from Elsevier); bottom: scanning electron microscopy (SEM) images of LIG pattern on pristine and copper-coated Nomex sheet (reproduced from Ref. [54], Copyright 2021, with permission from the authors, licensed under CC BY 4.0). **e** Fabrication processes of the polyether ether ketone (PEEK)-based smart glove and its detailed SEM images. Reproduced from Ref. [56], Copyright 2022, with permission from Elsevier

materials, synthetic organic substances such as graphene oxide (GO) can be converted to reduced graphene oxide (rGO) [29, 30] or LIG [31] through the laser scribing processes. They have been used in flexible strain sensors [32] and flexible pressure sensors [33] (Fig. 3a). Although the above-mentioned industrially synthesized precursor materials [34–37] have excellent mechanical and electrical properties, they often exhibit poor biocompatibility and pose challenges to reusability, which renders them less environmentally friendly. To address these problems, researchers have recently shifted their focus toward developing LIG using easily obtainable natural materials, such as paper [38], cork [39], and lignin [40], and natural fiber materials such as cotton [41] and silk [42] (Fig. 3b). These natural materials offer advantages such as high carbon content, easy obtainability from natural sources, and reusability. As depicted in Fig. 3c, transforming natural materials into LIG requires optimization of the laser specifications and process conditions, because the photon energy absorption rate depends on the material. For example, lignocellulosic materials such as wood, paper, and textiles predominantly reflect near-infrared (NIR) light and strongly absorb ultraviolet (UV) light [43]. Owing to these properties, the use of laser wavelengths in the UV region has proved to be more effective in LIG generation because it efficiently induces photothermal reaction compared to NIR region [43]. Some heat-sensitive natural materials, such as silk and paper, can be carbonized via appropriate photothermal reactions to form graphene; however, inappropriate laser conditions may cause material damage. Consequently, careful optimization is needed to ensure the safety of these materials [42]. Because natural material-based LIG is highly biocompatible and cost-effective, current studies are developing functional devices that require biocompatibility [44] and mass production, such as skin-attached patch sensors [45].

Sensors having various functions can be created by producing graphene using only natural materials. However, better performance can be achieved by combining natural and synthetic materials [46]. Composites of natural and synthetic materials can be fabricated by mixing natural materials with polymers such as polydimethylsiloxane (PDMS) [47], aerosols [48], or GO nanosheets [49]. The mixture can then be coated onto a substrate and solidified [50] or molded into a fibrous membrane through electrospinning [51]. Films or fibrous membranes produced from appropriate mixtures are easily converted to graphene by promoting a carbonization reaction by laser writing technology, owing to the high carbon content of the natural material. When natural materials are used alone, problems such as low mechanical strength, low durability, or degradation by environmental factors such as moisture [38] occur; however, when they are mixed with synthetic materials, these problems can be overcome to achieve improved performance and multifunctionality.

Researchers are actively investigating the production of LIG-based wearable devices using advanced materials [52]. For example, Kevlar and polyvinyl acetate (PVA)/H_3PO_4 have been combined to create microsupercapacitors [53], and a glucose sensor was developed by electroplating copper onto a Nomex insulating sheet induced on graphene via a laser [54] (Fig. 3d). Moreover, research is being conducted on innovative LIG-based wearable devices using polyether ether ketone (PEEK) [55], which is an engineering plastic; through this research, products such as wearable gloves that are capable of self-power generation and touch sensing are being developed [56] (Fig. 3e). The optimal conditions and wavelengths for the LIG formation from various materials are summarized in Table 1.

Simultaneous material transformation

In addition to the facile preparation of LIG from various organic materials, a composite configuration of LIG with certain nanomaterials can be readily fabricated by introducing mixed organic precursors for simultaneous material transformation [57, 58]. The composite precursors can be prepared by blending nanomaterials with polymer bases such as poly(amic acid) (PAA) [59] and polybenzimidazole (PBI) [60] before solidification or by directly coating them onto the substrate [61, 62]. Although the preprocessing is somewhat different, the precursors eventually form planar mixed films through coating and baking procedures to furnish LIG/nanomaterial composites with a single scan of a focused laser (Fig. 4a). Compared with the standalone use of LIG, the resultant nanocomposite with new materials has significantly better inherent performance [63] or unique characteristics [64] that exceed the innate versatile functionality of LIG [65]. The reported nanocomposites generally consist of a heterogeneous structure with low-dimensional materials (LDMs) embedded in them; these LDMs are highly recognized for their excellent properties [66], such as large surface area, ultralight weight, high reactivity to surrounding environments, and superior mechanical strength with flexibility. Regardless of their morphological diversity, all types of LDMs are compatible with selective laser processes for simultaneous material transformation, including metal and metal–oxide [67–69] nanoparticles (NPs) in 0D, carbon nanotubes (CNTs) [70] in 1D, and MXene nanosheets [71] in 2D materials (Fig. 4b). These examples commonly use a single laser source to produce composite structures with conductive LIG channels and sensitive LDM nanomaterials for mechanical/chemical sensors and energy devices.

Although laser-induced material transformation is primarily a thermal process, the underlying heating mechanisms depend on the laser output operational mode, which is represented by a CW or pulsed laser. Currently, ultrashort pulsed lasers use a femtosecond (fs) repetition rate in pulse modulation, which minimizes heat transfer to the surroundings during laser irradiation [72]. In ultrafast photonic dynamics, when free electrons transfer energy to the lattice through electron–phonon collisions [73] under single-pulse irradiation, the target accumulates the generated heat through the multiphoton absorption effect of the fs laser pulses [74]. In contrast, the successive beam propagation of a CW laser generates a distributed temperature field, which is considered a heat-affected zone, via a photothermal effect that extends to the periphery of the irradiated spot through material heat transfer [75]. Thus, the difference in the photothermal-chemical reaction of each laser operational mode produces a distinct micromorphology in the resulting LIG/nanomaterial composite. As shown in Fig. 4c, the fs laser-processed area has a uniform graphene structure with ZnO particles remaining on its surface, whereas the CW laser-processed area contains irregular microstructures with aggregated ZnO clusters mixed into the carbon molecular skeleton. Therefore, relatively smooth LIG surfaces, which are capable of NIR light detection using the bolometric effect of graphene [76], and embedded ZnO, which is used for UV light detection through the photoconductive effect [77], facilitate the successful implementation of a dual-mode photodetector (PD) [78] (Fig. 4d). Notably, the introduction of multiple laser sources has proved their ability to effectively tune the function of a device, which is further discussed for advanced selective laser processes that are intended for all-laser technology.

However, mixing PI with stretchable organic substrates for wearable applications is important for adapting the intrinsic flexibility of substrates to brittle carbon products by completely integrating LIG into the substrate through concurrent carbonization. One of the most promising substrates for LIG integration is PDMS because its exceptional transparency,

Table 1 Optimal laser conditions for the formation of LIG in various materials

Type	Materials	Wavelength	Processing conditions	Reference
Synthetic materials	PI fabric	335 nm	20.5 mJ/cm^2, 100 mm/s	[19]
	cPI film	450 nm	1750 mW, 100 mm/s	[27]
	GO	1030 nm	330 mW, 125 mm/s, pulse duration 220 fs	[29]
	PEEK	532 nm	2.4 W, 100 mm/s, 500 kHz	[55]
Natural materials	Paper	532 nm	100 mW, 10 mm/s	[38]
	Cork	1.06 μm	5.5 W, 17.8 mm/s	[39]
	Cotton	10.64 μm	0.6 J/mm^2	[41]
	Silk	1064 nm	0.2 W, 30 mm/s, 20 kHz	[42]
	Leaf	346 nm	350 mW, 10 mm/s, 201.5 kHz, pulse duration 255 fs	[43]
Hybrid materials	Cellulose nanofiber	10.6 μm	3.6 W, 10 mm/s	[46]
	PDMS/lignin composite	355 nm	1.2 W, 40 mm/s	[47]
	RF aerogel	400–460 nm	3 W, 0.2937 mm/s	[48]
	Lignin paper	460 nm	460 mW, 303 mm/s	[50]
	Lignin/PAN fiber	450 nm	1 W, 100 mm/s	[51]

LIG: laser-induced graphene; PI: polyimide; cPI: colorless polyimide; GO: graphene oxide; PEEK: polyether ether ketone; PDMS: polydimethylsiloxane; RF: resorcinol–formaldehyde; PAN: polyacrylonitrile

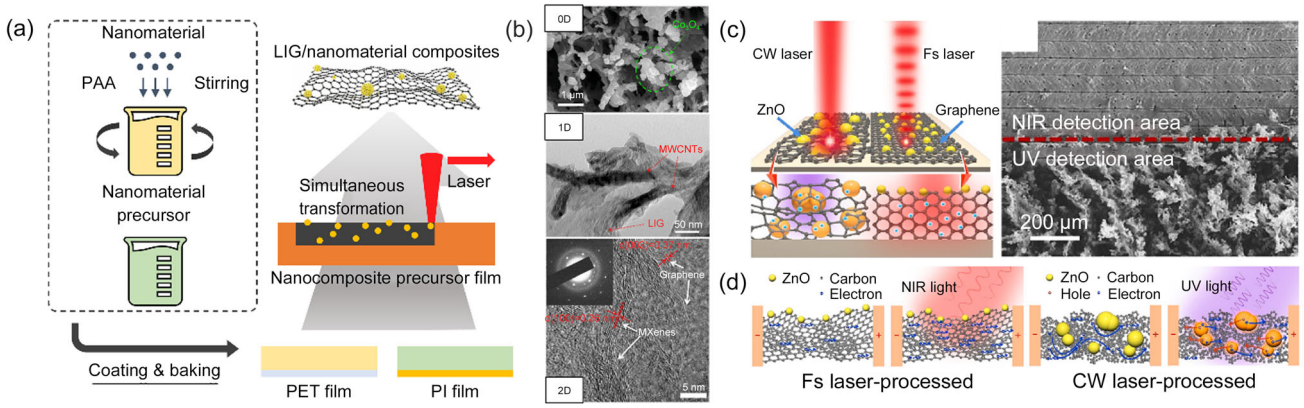

Fig. 4 **a** Schematics of processing steps for simultaneous material transformation to obtain laser-induced graphene (LIG)/nanomaterial composites. Reproduced from Ref. [60], Copyright 2022, with permission from Elsevier. **b** Scanning electron microscopy (SEM) and transmission electron microscopy (TEM) images of low-dimensional (0D, 1D, and 2D) materials integrated into the 3D LIG structure. The top one is reproduced from Ref. [69], Copyright 2022, with permission from Elsevier; the middle one is reproduced from Ref. [70], Copyright 2021, with permission from Elsevier; the bottom one is reproduced from Ref. [71], Copyright 2023, with permission from the American Chemical Society. **c** Schematic and an SEM image illustrating the difference between continuous-wave (CW) laser processing and femtosecond (fs) laser processing. **d** Near-infrared (NIR) light and ultraviolet (UV) light sensing mechanism of the fs laser-processed and CW laser-processed surfaces. Reproduced from Ref. [78], Copyright 2023, with permission from Elsevier

stretchability, and biocompatibility are ensured [79]. The PI/PDMS composite with specifically designed LIG electrodes exhibits adequate electrical properties and durable mechanical robustness for use in skin-attachable strain sensors [80, 81]. Furthermore, paper- and cloth-integrated LIG circuits [82] show significant potential as functional building blocks, such as packaging components and fabric fibers for smart wearable electronics.

In conclusion, we have discussed the simultaneous material transformation of the mother substrate, as well as nanomaterial precursors to create functional LIG-based nanocomposites with a single scan of a laser. Together with the enhanced mechanical and chemical properties of the resultant composites, simple variations in the laser source or preprocessing methods produce novel characteristics for advanced applications. Although the laser-induced simultaneous material transformation technique shows notable

outcomes for the fabrication of functional elements, the need for the proper support for additional processing steps or the manual implantation of supplementary units to design multilevel configurations for system-level wearable devices is a considerable challenge. However, we expect that the integration of multiple laser-induced transformative processes may be a breakthrough for the current challenges by direct writing of functional layers as mentioned above.

Consecutive multilayer configuration

Based on precisely patterned LIG layers, functional multilayers are assembled by consecutively stacking on-demand materials to satisfy the requirements for successful device operation. In the simplest cases, the LIG pattern functions as a conductive electrode or multifunctional element, and the applied functional materials are responsive to the intended stimuli, whereas the encapsulation layers are selectively added to protect the entire system if needed. The well-known applications are energy devices, environmental sensors, and health monitoring systems with selected biocompatible materials, as listed in Table 2. The aforementioned research highlights the flexibility and stretchability of the demonstrated devices as a proof-of-concept for wearable applications and the guaranteed scalability of the LIG-based multilayer configuration for extra components, including electronic and mechanical systems.

More advanced attachable sensing devices feature highly sophisticated multilayer circuit configurations for use in multimodal sensor networks and wireless communication. Figure 5a shows a flexible plant growth monitoring system that comprises a temperature sensor, an optical sensor, and two humidity sensors for the real-time measurement of environmental temperature, light irradiation intensity, and humidity [103]. The screen-printed Ag and LIG electrodes functionalize each sensor, when combined with $ZnIn_2S_4$ (ZIS) nanosheets or SnO_2/CNT films, and work as conductive channels to interconnect the electronic elements. Because of the cellular structures of the porous LIG electrodes, which are depicted in the detailed schematic of the integrated device, the active humidity sensing of ambient humidity and leaf transpiration are monitored owing to the absorption and desorption of water molecules (Fig. 5b). Another advantage of the fully integrated sensing chip system is the improved applicability in versatile multiscenario situations. A Ag/MXene sponge incorporated into the LIG-based interdigitated electrode enables a fully integrated wireless pressure-sensing chip system comprising a flexible printed circuit board with various electronic chip components, including capacitors, resistors, and data transmission antennas [104] (Fig. 5c). Figure 5d depicts the applications of the proposed attachable pressure sensor in different scenarios, such as fruit cultivation, joint movement, and pulse signals that show promise for next-generation wearable devices.

Beyond the progress of functional electronic circuit designs, the implantation of individual rigid systems on wearable scaffolds, implemented through the selective patterning of LIG on flexible PI films, enables a high level of biomedical signal analysis. For example, a heterogeneous combination of narrowband vertical-cavity surface-emitting lasers (VCSELs) and a Si PD unit on a flexible Au-LIG hybrid electrode formed an epidermal biocompatible optoelectronic sensor for health monitoring [105] (Fig. 5e). On the surface of the skin, VCSELs emit lasers in separate wavelengths that are reflected to the PD after passing through a blood vessel, which gathers health data from the wearer, such as blood oxygen level and pulse rate (Fig. 5f). Moreover, for reliable medical diagnostics through the analysis of human sweat, composite data containing multiple chemicals in human sweat are required, whereas conventional wearable sweat sensors cannot provide valuable detection because studies have only focused on proof-of-concept designs rather than considering the practical applications. For the scalable and accurate use of the sweat sensor, a microfluidic chamber is installed to supply consistent and uncontaminated sweat volumes to the LIG-based sweat sensor, thereby enabling continuous multisubject analysis of both sweat metabolites and electrolytes [106] (Fig. 5g). As shown in Fig. 5h, the real-time responses of the on-body glucose, lactate, and sodium levels were investigated during cycling to monitor physical state of the wearer. These reports emphasize the need for consecutive multilayer configurations in basic LIG electronics for feasible applications in wearable devices by introducing functional materials, advanced circuit designs, and adaptable systems.

The consecutive multilayer configuration method reinforces the functional elements of devices and evades innate mechanical fragility. This offers unrivaled capabilities for wearable technologies. Recent studies continue to validate the effectiveness of multiple integrations of LIG with the following components: specifically designed electronic circuits and encapsulation layers [107], stretchable elastomeric substrates, and dielectric functional materials [108]. In summary, the major advantage of LIG in the multilayer film system is unlimited scalability; this is achieved by establishing a basic integrative platform with multifunctional variability that can consolidate diverse units to fully configure system-level standalone devices.

Conventional laser process

As discussed in the preceding sections, transformative approaches, including LIG, have initiated a new and significant research direction and have successfully generated

Table 2 Representative applications of multilayered laser-induced graphene (LIG) devices

Type	Multilayered materials	Application	Reference
Energy device	Poly(3,4-ethylenedioxythiophene) (PEDOT)	Supercapacitor	[83]
	Phosphor Cu	Supercapacitor	[84]
	Glucose dehydrogenase-bilirubin oxidase	Biofuel cell	[85]
	Graphene oxide (GO)	Triboelectric nanogenerator (TENG)	[86]
	Reduced graphene oxide (rGO)	Pressure sensor-integrated TENG	[87]
Mechanical and chemical sensors	Co nanoparticles	Strain sensor	[88]
	Ag electrodes with kirigami design	Strain sensor	[89]
	GO	Humidity sensor	[90]
	Pd/HNb_3O_8	Humidity sensor	[91]
	MoS_2	Gas sensor	[92]
	Polydimethylsiloxane (PDMS)	Moisture-resistant gas sensor	[93]
Skin-interfaced monitoring system	$ZnIn_2S_4$ (ZIS)	Skin moisture sensing	[94]
	Functional polymer layers	Sweat sensor	[95, 96]
	Embedded metal nanoparticles	Sweat sensor	[97–102]

numerous research outcomes. The inherent versatility of LIG has been proved, and it has been applied across various fields. As outlined earlier, various research activities, such as design optimization, raw material exploration, and the introduction of additional materials, are being undertaken to further expand the potential application and performance of LIG. However, a wearable device may consist of multiple components that may have sophisticated the fabrication of multilayer structures. The transformative approach may provide a solution to specific constituent elements; however, LIG alone is not sufficient for the complete fabrication of a whole device. In this regard, existing laser processes have also consistently advanced with the development of wearable devices. These methods are categorized as conventional approaches because they involve laser processes that were established before the emergence of the transformative approach. They can be further categorized into subtractive approaches, where the material is removed from the investigated area by lasers, and additive approaches, where material is generated in a designated region through laser-induced processes. Laser texturing includes methods that specifically focus on surface processing and involve both additive and subtractive approaches. Laser processes that are difficult to categorize within these defined categories are summarized in a separate section.

Laser ablation/machining

The selective removal of materials using lasers has distinct advantages over other standard techniques of fabrication, particularly for unconventional materials [9] having complex compositions or other emerging materials that require rapid prototyping for proof-of-concept wearable devices. Thus, laser ablation is an effective patterning scheme for low-dimensional nanomaterials and their nanocomposites that have been extensively investigated as constituents in flexible and stretchable applications. Nanomaterials and nanocomposites have been recently introduced and include Cu–Au core–shell nanowires (NWs) [109], Ti_3C_2 − MXene [110], poly(diallyldimethylammonium chloride) (PDDA)-modified rGO with exfoliated $Ti_3C_2T_x$ [111], poly(3,4-ethylenedioxythiophene):poly(styrene sulfonate) (PEDOT:PSS) with aramid nanofibers [112], multiwalled carbon nanotube (MWCNT)/PDMS composites [113], and MWCNT–MnO_2 films [114], which are now compatible with laser patterning techniques using conventional ablation mechanisms. Most of these new materials can be removed at a microscale resolution with clean boundary features and minimal damage to the underlying substrate when laser parameters are optimized, as shown in Fig. 6a. The modifiable thickness by ablation is on the order of about 100 nm for the NW percolation network membrane [109], yet laser ablation is compatible with a considerably thicker target layer, even up to several hundreds of micrometers [111]. The

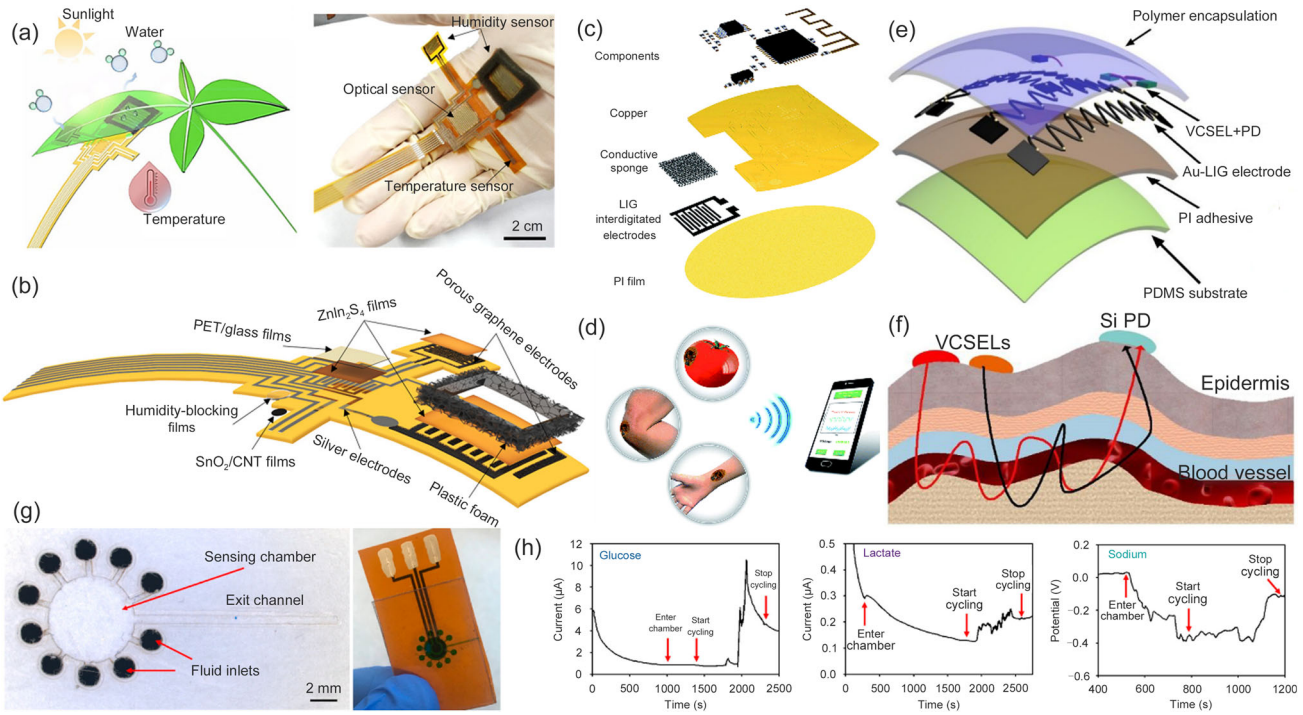

Fig. 5 **a** Schematic and a digital image of a flexible plant growth monitoring system. **b** Detailed configuration of the multimodal plant healthcare flexible sensor system. Reproduced from Ref. [103], Copyright 2020, with permission from the American Chemical Society. **c** Multilayered integration of the attachable strain sensing system. **d** Multifunctional applications of sensor chip and wireless communication. Reproduced from Ref. [104], Copyright 2021, with permission from The Royal Society of Chemistry. **e** Complete configuration of a skin-interfaced optoelectronic device. **f** Schematic of the blood oxygen sensing mechanism. Reproduced from Ref. [105], Copyright 2022, with permission from the American Chemical Society. **g** Digital images showing the design of a microfluidic chamber and its integration with a patterned laser-induced graphene (LIG) sweat sensor on polyimide (PI) film. **h** Real-time on-body monitoring of glucose, lactate, and sodium levels during cycling. Reproduced from Ref. [106], Copyright 2023, with permission from the American Chemical Society

as-prepared patterned layer often undergoes additional processing, such as electroplating [114], transfer to other thermal plastic films [111], or direct attachment to the human body [109], for use in electrophysiological sensors that monitor human motion or as energy sources for the standalone operation of other wearable devices.

Facile patterning enabled by laser ablation makes possible rapid design changes, which also results in changes in device performance, as was observed for a microsupercapacitor with electrodes connected in parallel and in series for different working voltages [112]. The working voltage can also be changed by applying a laser process to the electrolyte layer instead of modifying the electrode design [57]. In addition to its patterning capability, laser ablation has advanced in multiple directions. Laser ablation can affect the performance of the resultant device even without a design change, as confirmed by a study on the laser ablation of MWCNT/PDMS composites [113]. The cross-sectional morphology of a laser-ablated sample, and hence the resultant conductive network, was adjusted through the laser conditions used for the ablation process, which was also closely related to the gauge factor of the final strain sensor (Fig. 6b).

An in-depth study of other specific ablated targets, such as graphene films having 6–8 layers [115], also demonstrated that different ablation patterns may result in distinct working mechanisms for different uses in device fabrication. The number of applicable materials is continuously increasing; applicable materials now include uncommon microbial conductive biofilms such as *Geobacter sulfurreducens* for electricity generation from water evaporation [116]. From the perspective of applications, thin-film thermoelectric (TE) generators and stretchable batteries have been developed by patterning TE materials in a zigzag pattern [117] and separating lithium titanium oxide (LTO) anodes and lithium iron phosphate (LFP) cathodes into independent microscale square arrays [118] (Fig. 6c) based on the site selectivity of the direct laser ablation technique. These studies have successfully broadened the range of laser-enabled wearable energy devices and have focused mostly on microsupercapacitors.

Although laser ablation is increasingly being used on new materials, the mechanism behind it remains ambiguous and

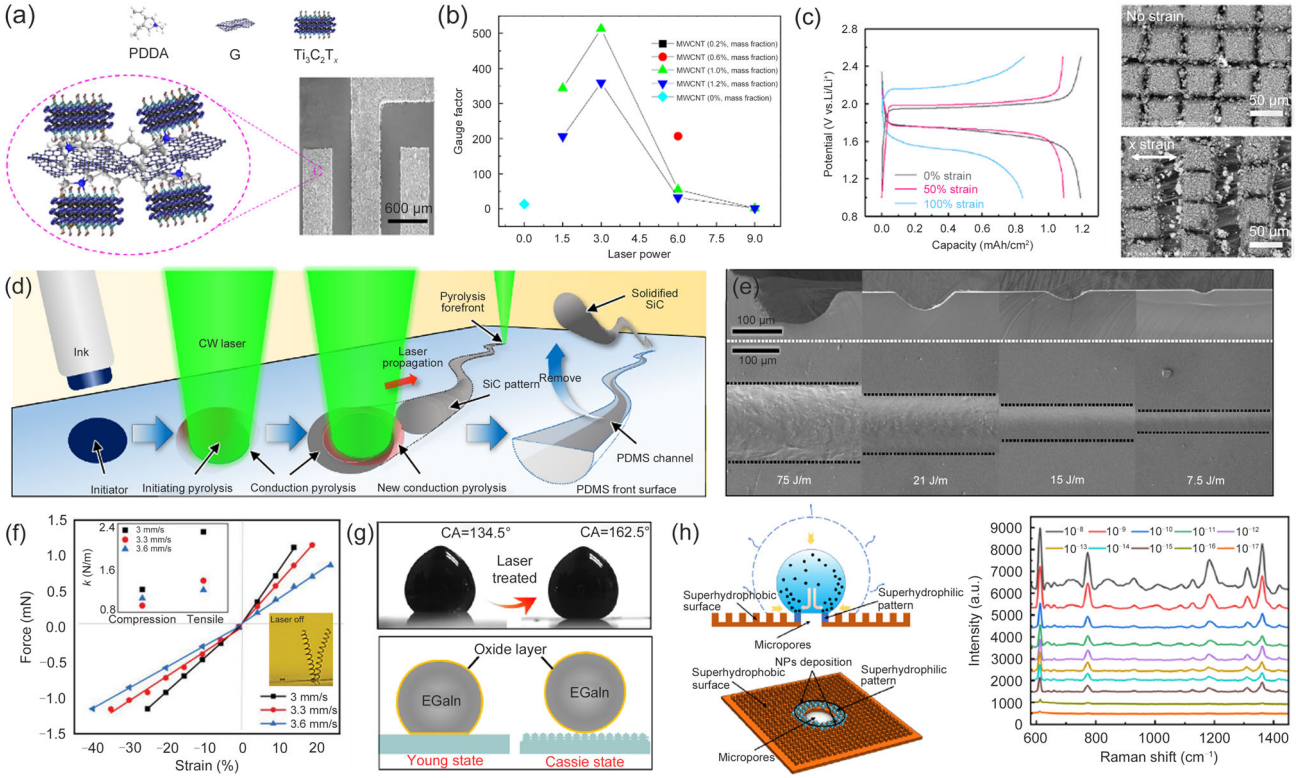

Fig. 6 **a** Clean ablation of poly(diallyldimethylammonium chloride) (PDDA)-modified reduced graphene oxide (rGO) with exfoliated $Ti_3C_2T_x$. Reproduced from Ref. [111], Copyright 2022, with permission from Elsevier. **b** Gauge factor of multiwalled carbon nanotube/polydimethylsiloxane (MWCNT)/PDMS with different MWCNT contents processed at various laser powers. Reproduced from Ref. [113], Copyright 2020, with permission from Elsevier. **c** Discharge/charge voltage profiles of laser-processed stretchable battery in different stretched states (right: scanning electron microscopy (SEM) images of stretchable lithium titanium oxide (LTO) electrodes under different strains). Reproduced from Ref. [118], Copyright 2022, with permission from Elsevier. **d** Schematic illustration of the successive laser pyrolysis (SLP) process for PDMS micromachining. **e** Cross-sectional and top-view SEM images of PDMS after SLP micromachining. Reproduced from Ref. [126], Copyright 2020, with permission from the authors, under exclusive license to Springer Nature Limited. **f** Force–strain curve of laser-induced graphene (LIG) spring created by the pyrolytic jetting process. Reproduced from Ref. [128], Copyright 2023, with permission from the authors, licensed under CC BY. **g** Contact angles of an EGaIn droplet on a polyvinyl acetate (PVA) surface before and after laser texturing. Reproduced from Ref. [141], Copyright 2020, with permission from the American Chemical Society. **h** A surface-enhanced Raman spectroscopy (SERS) sensor on laser-textured copper film (left: schematic of the evaporation process; right: Raman spectra of rhodamine 6G (R6G) at different concentrations). Reproduced from Ref. [149], Copyright 2022, with permission from the American Chemical Society

involves diverse interactions and feedback between the incident light and the target material [9]. In contrast, recent studies on the laser micromachining of specific substrates have described attractive two-step approaches that incorporate a transformative step before the removal of material. It remains unclear which class of substrate is compatible with the corresponding approach; however, meaningful results have been observed for PDMS and PI, which are both valuable materials for wearable device applications. Note that conventional laser ablation techniques are still extensively used for the relevant polymer materials [119] to create various on-demand patterns, including quasi-3D patterns [120–122] and rapid prototypes of user-defined microfluidics channels [123, 124]. However, owing to difficult-to-control ablation phenomena, conventional laser ablation using a pulsed laser generally yields poor surface quality with residual burrs and debris around the processed area, even with ultrashort lasers [125]. In contrast, a recently developed patterning technique for PDMS [126] uses seamless photothermal pyrolysis conducted using a CW laser, which converts PDMS into SiC along the laser scanning path. Although PDMS is highly transparent at visible wavelengths, a 532 nm green laser is used to induce selective pyrolysis with the aid of successive laser pyrolysis (SLP), which relies on an iterative change in laser absorption and a subsequent increase in heat transfer to the vicinity upon the conversion of PDMS to SiC. The resultant SiC is then simply removed using mechanical methods, such as ultrasonication, to complete the nonablative PDMS machining process, as shown in Fig. 6d. The resultant PDMS

after machining does not exhibit an exceptional surface morphology (Fig. 6e) but retains its original surface chemistry, which is essential to customizing organ-on-a-chip applications. The nonablative micromachining technique for PI substrates [127] holds equivalent problems to that of PDMS, but two major differences are observed. The product created from the laser-induced pyrolysis of PI is LIG, which can be exfoliated spontaneously from the original matrix owing to the intensive gas emission at the laser spot under scanning. This "pyrolytic jetting" technique not only enables direct micromachining of the PI substrate but can also be used to create 3D LIG helical springs [128] (Fig. 6f) through a minor experimental modification, which is expected to be useful for multifunctional electromechanical systems, as confirmed from its strain–force characteristics.

From a practical perspective, laser equipment has become more widely available and has emerged as an efficient tool for rapidly creating proof-of-concept wearable devices. Consequently, the use of laser machining continues to increase, even on conventional materials. For instance, the laser ablation of Cu thin films to achieve specific patterns, e.g., a serpentine pattern, enables rapid feasibility testing of stretchable wearable applications such as thermo-haptic devices [129] and multispectral active cloaking devices [130]. We also found an indirect application of Cu as a mold after it was laser machined into microcone cavities for a sensitivity-tuned pressure sensor [131]. In addition to these activities, the laser process has been integrated with different types of industrialized materials for wearable applications, such as denim fabrics [132] and textiles [133], for automated, data-driven mass production of real-world wearable devices. In a recent study, the authors created a multifunctional sensor on nylon textile by functionalization with GO via a two-step wet process and selective laser reduction while consecutively integrating Ag NPs into the resultant rGO/textile composite through laser-driven photoreduction to obtain antibacterial properties [134]. Meanwhile, theoretical and experimental studies on the development of novel methods for the laser-selective removal of multilayer materials are actively being conducted [135].

Laser texturing

Laser texturing can be applied to manipulate diverse physical and chemical properties, including optical [136], electrical [137], and mechanical characteristics [138], as well as biological compatibility [139]. However, laser-induced wettability control and laser-enabled surface-enhanced Raman spectroscopy (SERS) templates are two areas in which significant developments, from the perspective of wearable technology, were presented after 2020, due to the emergence of highly sensitive chemical and molecular sensors for the wearer. In particular, laser texturing is a facile and effective method for changing the wettability of a target material by modifying its surface properties [140]. Recent studies have shown that laser-induced wettability control enables the direct patterning of liquid metal without injecting the fluid into a predefined microchannel, which is the most widely used method for fabricating EGaIn-based stretchable devices. When fs laser microfabrication was used on a PVA substrate, a supermetalphobic area based on a porous network of micro/nanostructures was created [141, 142], whereas the functional groups of the PVA remain unchanged. Owing to their modified surface morphology, the oxide layer of EGaIn and PVA, which was originally in Young's state, changed to the Cassie state with a contact angle of 162.5°, as shown in Fig. 6g. Consequently, EGaIn was printed only on the pristine PVA without laser texturing upon brushing. An additional advantage of the resultant EGaIn electronics is that the circuit can be repaired or even reconfigured via rebrushing the EGaIn droplets. Wettability control by laser texturing can also provide new functionality or enhance the performance of the final device, as was observed for the texturing of a double-sided micropyramid on PDMS using a laser [143]. Laser-induced surface texturing enables the patterning of a functional layer, without changing its wettability, using a polyethylene (PE) film as a supplementary layer to create grooves in the target substrate [144]. Laser texturing is also compatible with other laser processes; by applying laser texturing to LIG, a nonstick conductive structure for Galinstan droplets by nonwetting characteristics was created to develop a tilt sensor that could distinguish various slanting orientations [145].

Surface texturing can be crucial for some applications; a representative example is SERS, which enables the high-precision detection of target molecules [146, 147]. SERS techniques are expected to be vital for wearable healthcare devices and sensors for real-time diagnosis and the detection of potential threats. Recent studies have shown that laser texturing enables the successful fabrication of efficient SERS templates. Because a sensitive SERS template should be able to acquire Raman signals from a highly diluted solution, the coffee-ring effect after evaporation of containing liquid should be suppressed by controlling the contact angle (CA) and sliding angle within the appropriate ranges, which is achieved using the fs laser texturing of an AISI304 stainless steel sheet by creating nanoscale rough surface [148]. A more advanced version of the wearable SERS template was created on a 0.1-mm Cu foil by creating superhydrophobic/superhydrophilic hybrid structures with micropores at their centers using a laser to precisely deposit the target material at the designated area, as shown in Fig. 6h [149]. The resultant SERS template was able to detect target molecules, even at the attomolar level, and demonstrated the great potential of selective laser texturing techniques for highly sensitive biosensors. Furthermore, the facile and robust laser-enabled

SERS platform was implemented as single-step laser patterning to integrate plasmonically active Ag clusters into a flexible polymer [150]. The resultant platform successfully detected subtle changes in its vibrational spectrum after being functionalized with 4-nitrobenzenethiol and exhibited superior resilience against mechanical disturbances. The major advantages of laser-enabled SERS platforms are that laser texturing is compatible with irregular substrates and additional processing. This confirms that selective laser processing introduces new possibilities for on-demand multifunctional SERS platforms [134].

Sintering and synthesis

As mentioned in the previous section on laser ablation/machining, nanomaterials are an important class of materials for use in wearable devices. Laser technologies, such as sintering and synthesis, have been investigated in relation to the efficient use of these materials in additive processes [11]. Owing to the large surface area exhibited by nanomaterials, noble metals—Ag NPs and NWs in particular—have been the focus of research due to their noncorrosive and nonoxidative characteristics, and a considerable portion of the recent research can be considered an extension of this trend [151, 152], which is supported by their originality. To date, most laser processing has been applied to flat surfaces, even for flexible and stretchable applications; however, Ag NP laser sintering has recently been conducted on different types of substrates, such as polyvinylidene fluoride (PVDF) monofilament fibers, having circular cross sections [153]. Moreover, donor and acceptor substrates can be differentiated to increase the type of polymer substrates that are applicable to the laser sintering process [154]. Laser sintering has also become more compatible with advanced applications such as data-driven motion sensors and multifunctional skin electronics [155, 156]. In addition to this overall progress, selected publications representing two different development perspectives will be introduced as follows: the modification of the sintering process and the introduction of additional emerging materials.

Laser sintering has been applied to various metal NPs, and analogous reductive sintering processes have also been reported for several metal–oxide NPs, such as CuO and NiO NPs, thereby enabling the facile generation of electrodes at the microscale. Thus, monolithic laser reductive sintering (m-LRS) was proposed by making a minor change to the reductive sintering process of NiO NPs [157]. Hatch scanning is generally used to fill in a designated area to create a planar electrode; however, several scanning lines were intentionally skipped during the hatch-scanning procedure to create a NiO channel between the two Ni electrodes, as shown in Fig. 7a. Consequently, a Ni–NiO–Ni structure was created to produce a negative temperature coefficient (NTC) thermistor (Fig. 7b). This resistance response is different from the typical temperature dependency of the Ni electrode, which exhibits a positive temperature coefficient of resistance. Interestingly, the B-value of the resultant Ni–NiO–Ni structure was calculated to be 7350 K and as high as 8162 K near room temperature. These values are among the highest sensitivities for thermistor-based temperature sensors, and such superior sensitivity may be attributed to the rapid thermal annealing at the NiO channel, which results in decreased nickel vacancies. The demonstration of Ni–NiO–Ni as a wearable epidermal temperature sensor demonstrates the contribution of the m-LRS process to the development of ultrathin wearable, flexible devices.

Among the relevant materials, EGaIn has been favored for laser sintering. First, the liquid metal is prepared as a discrete droplet that is compatible with the laser sintering scheme [158]. In droplet form, the liquid metal can be directly patterned onto the target substrate; however, Ag NWs have been introduced in addition to enhanced adhesion between the target material and tunable electrical properties [158]. EGaIn particles (EGaInPs) with Ag NW additives (AgNWs-EGaInPs) form a stable film when the vacuum filtration and transfer method are used, whereas EGaInPs alone result in a poor-quality film. The as-prepared Ag NWs-EGaInP film is composed of physically mixed EGaInPs and Ag NWs, but their level of entanglement can be controlled by subsequent laser irradiation. This entanglement structure creates a strain-insensitive electrode, which is crucial for wiring purposes and freestanding patterned liquid metal thin-film conductors (FS-GaIn) [159]. Another study further confirmed that a freestanding liquid metal–AgNW composite thin film can be useful as an electrical connection between the chip and conductor [160], but mechanical disorder of stiff chip and stretchable conductor remains a major limitation for wearable devices. When the prepatterned freestanding stretchable soldering sticker (STicker) is soldered between the two conductors, the corresponding sticker can be stretched up to 5 mm, as shown in Fig. 7c.

Considering these developments, laser sintering is becoming a mature technology that is now compatible with wearable devices of higher complexity. A representative example of this trend is the Ag NW and thermochromic liquid crystal (TLC)-based artificial chameleon skin (ATACS) [161], which was recently developed for the rapid coloration of skin into a surrounding habitat with diverse colors, as shown in Fig. 7d. A closer examination of its structure reveals that the device is composed of dense multilayers connected via the laser sintering of Ag NPs. For a more site-specific, locally confined use of nanomaterials, laser-induced synthesis has been investigated for multiple NWs on flexible substrates [162]. For wearable device applications, two different types of NWs, p-CuO NW and n-ZnO NW, have been consecutively synthesized using a laser-induced hydrothermal growth scheme

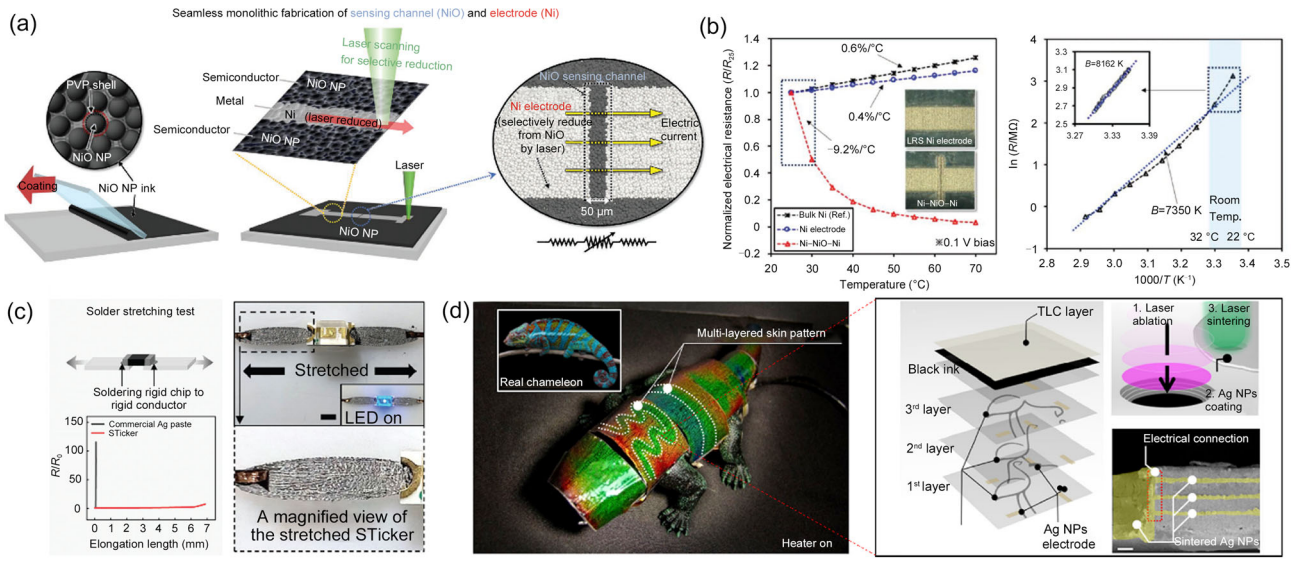

Fig. 7 **a** Monolithic laser reductive sintering (m-LRS) process for monolithic Ni–NiO integration. **b** Temperature-dependent electrical resistance showing negative temperature coefficient (NTC) behavior and an unprecedentedly high B-value. Reproduced from Ref. [157], Copyright 2019, with permission from the authors, licensed under CC BY. **c** Solder stretching test for STicker wistretching testth its optical photographs. Reproduced from Ref. [160], Copyright 2023, with permission from Wiley–VCH GmbH. **d** A biomimetic chameleon soft robot (left: Ag NW and thermochromic liquid crystal (TLC)-based artificial chameleon skin (ATACS) patch in operation; right: configuration of multilayered ATACS). Reproduced from Ref. [161], Copyright 2021, with permission from the authors, licensed under CC BY 4.0

to create a highly efficient UV microphotodetector compared with homojunction of CuO–ZnO structures [163]. Moreover, efforts continue to synthesize new target materials, such as SiC [164] and Pd-$WO_3 \cdot xH_2O$ microwire [165].

Others

Lasers are flexible tools that enable various photothermal, photochemical, and photophysical reactions. Consequently, the use of lasers has been continuously increasing in recent studies. Recent examples that are relevant to wearable devices include indium zinc oxide (IZO) annealing [166], the curing of water-soluble polymers [167], sol–gel transition [168], metal textile welding [169], cPI lift-off [170], and photoresist (PR) patterning [171]. In many studies, lasers simply provide a facile substitute treatment for the conventional method compared with that fabricated by other processes, while also providing improved performance. Figure 8a shows the photocurrent density of hematite nanorod (NR) photoelectrochemical cells as a function of the applied potential after different annealing processes. Thermally annealed hematite NR (TAHN) exhibits inferior performance to laser-annealed hematite NR (LAHN), even at a high annealing temperature of 800 °C. This study proved that the laser technique is an alternative to the conventional counterpart and has the potential to significantly improve the resultant device performance.

Innovative laser processes are continually being reported, and some selected works that are relevant to wearable devices are summarized in this section. One specific form of material that is valuable for wearable devices is fibers for fabrics and textiles, and the thermal drawing technique (Fig. 8b) enables the integration of multiple elements such as tin selenide (SnSe) TE material into an arbitrary fiber. In contrast, the performance of the as-prepared TE fiber as a TE device is unsatisfactory because of its polycrystalline nature. Thus, a laser is an appropriate tool for inducing the continuous crystallization of a thermally drawn fiber into a single-crystal SnSe fiber [172]. Laser crystallization successfully improved the ZT value of single crystal to 2, as shown in Fig. 8c, which is comparable to the best ZT value for bulk TE materials. In addition, the mechanical properties of the SnSe fibers were compatible with wearable device applications. Similarly, laser photothermal reactions can produce unique results, depending on the material under consideration, and are often accompanied by additional processes or specific configurations. For Cu NWs, laser oxidation/reduction is combined with wet oxidation to achieve a reversible selective laser-induced redox (rSLIR) cycle, which successfully creates a multispectral monolithic PD that exhibits unique responses to RGB signals (Fig. 8d). Regarding the specific configuration, the laser-induced photothermal reaction at the PI/PDMS interface revealed that adhesive-free bonding may occur because of the enhanced mechanical interlocking at the

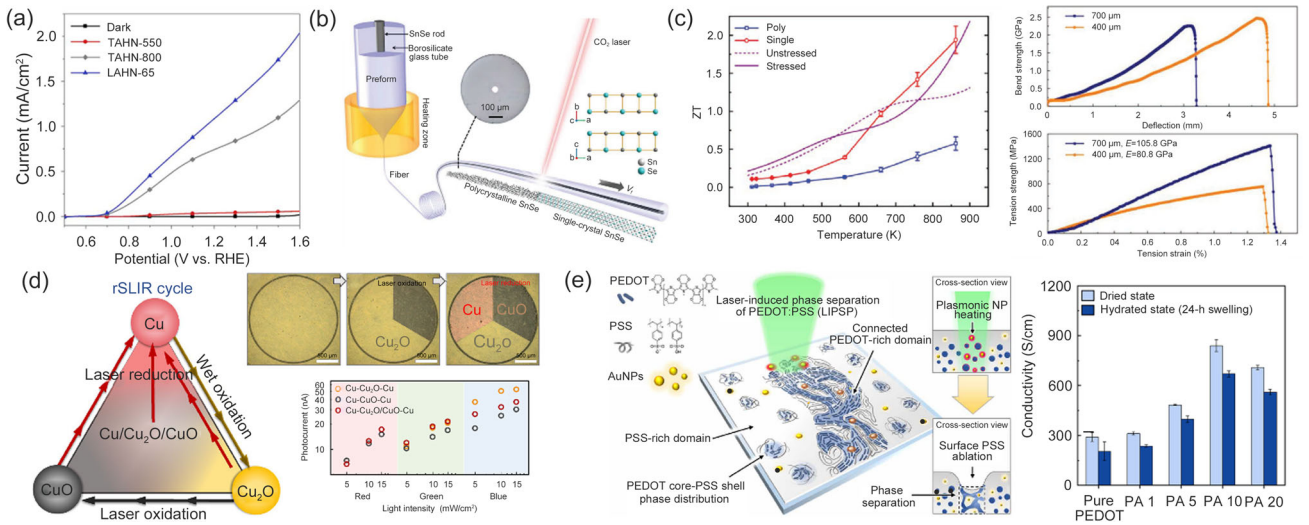

Fig. 8 **a** Photocurrent density of photoelectrochemical (PEC) cells after thermal and laser annealing. Reproduced from Ref. [175], Copyright 2020, with permission from the American Chemical Society. **b** Schematic illustration of thermal drawing and laser crystallization of SnSe fiber. **c** Thermoelectric figure of merit ZT value of poly- and single-crystal SnSe fibers and their mechanical properties. Reproduced from Ref. [172], Copyright 2020, with permission from WILEY–VCH Verlag GmbH & Co. KGaA, Weinheim. **d** Diagram of the reversible selective laser-induced redox (rSLIR) cycle and photocurrent level for different laser-enabled material configurations. Reproduced from Ref. [176], Copyright 2022, with permission from the authors, licensed under CC BY 4.0. **e** Schematic illustration of the laser-induced phase separation of poly(3,4-ethylenedioxythiophene):poly(styrene sulfonate) (PEDOT:PSS) and its electrical conductivity in the dried and hydrated states. Reproduced from Ref. [174], Copyright 2022, with permission from the authors, licensed under CC BY 4.0

microscale [173]. Laser irradiation of PEDOT:PSS [174], in contrast, reveals that phase separation occurs to separate the connected PEDOT-rich and PSS-rich domains, as shown in Fig. 8e, which results in a highly conductive water-stable hydrogel. These latest studies suggest that laser processing is not only useful for wearable devices but can also enable innovations in bioimplantable devices.

Applications

In the previous section, we discussed the latest developments in selective laser processes for wearable technologies by focusing on the patterning of multifunctional LIG with compatible nanomaterials, the integration of sophisticated electromechanical systems to fabricate advanced functional devices, and the use of conventional laser techniques for feasible industrial applications. Several technologies intended for wearable applications have been achieved—at least to the proof-of-concept level—through the corresponding laser processes. The two most important categories of these laser-enabled wearable applications are sensors and energy devices, which indicates that the primary goal of wearable devices is to detect human motion and physiological data in a remote, self-operative manner. The latest research on these sensors and energy devices is summarized in the tables in terms of the relevant laser process, laser source, materials of concern, and resultant performance. Sensors can be subcategorized as chemical sensors, which analyze components such as body fluids or monitor the surrounding environment for gasses and humidity (Table 3), and physical sensors, which respond to other factors such as strain and pressure (Table 4). Energy devices include energy harvesting devices, such as TE devices and TENGs, and energy storage devices, such as supercapacitors and batteries (Table 5).

Furthermore, emerging all-laser fabrication strategies, which are considered the ultimate goal of selective laser processes by encompassing the broad advantages of individual laser-based methods, are important for their notable impact on systematic laser processing in wearable device configurations. In this section, several advanced system-level studies are categorized into two representative methods: multistep laser processing by sequentially combining laser processes and multilaser processing through the use of separate laser sources.

Multiple laser processes

With no complicated mechanical machining or restrictive chemical treatments, the all-laser-driven fabrication method successfully delivers useful outcomes that can replace time-consuming procedures and toxic chemicals. As an example, the sequential fabrication of an on-body sweat sensor, a resistive temperature sensor, and a piezoresistive strain sensor

Table 3 Chemical sensors

Application	Laser process	Laser source	Materials	Performance	Reference
Sweat sensor	LIP	450 nm laser	Paper	Sensitivity: 0.08 $\mu A \cdot \mu M^{-1} \cdot cm^{-2}$; LOD: 0.14 μM	[82]
	LIP	CO_2 laser	PI film	Sensitivity: 2040 $\mu A \cdot mM^{-1} \cdot cm^{-2}$; LOD: 0.29 μM; Linear range: 0.5–1666 μM	[101]
	LIP	CO_2 laser	Metal + LIG composite	Linear range: 1–100 μM; LOD: 0.47 μM	[102]
	LIP and laser cutting	CO_2 laser	PI film	Sensitivity: 2.47×10^{-3}; LOD: 220 μM; Linear range: 0.22–28 mM	[106]
	LIP and laser ablation	CO_2 laser	PI film + multilayer	Sensitivity: (UA) 3.50 $\mu A \cdot \mu M^{-1} \cdot cm^{-2}$; (Tyr) 0.61 $\mu A \cdot \mu M^{-1} \cdot cm^{-2}$	[177]
	Laser engraving	800 nm fs laser	PEDOT:PSS + carbon	Sensitivity: 0.875 $\mu A \cdot uM^{-1} \cdot cm^{-2}$; LOD: 1.2 μM; Linear range: 2–250 $\mu M \cdot L^{-1}$	[124]
	Laser engraving	CO_2 laser	$Ti_3C_2T_x$ MXene + LIG	LOD: 88 pM; Linear range: 0.01–100 nM	[178]
Glucose sensor	LIP	CO_2 laser	PI film + Pt NP coating + chitosan-glucose oxidase	Sensitivity: 4.622 $\mu A \cdot mM^{-1}$	[98]
	LIP	CO_2 laser	Nomex + Cu plated	Sensitivity: (CuO-U electrode) 0.25 $mA \cdot mM^{-1} \cdot cm^{-2}$; (Cu-MS electrode) 0.32 $mA \cdot mM^{-1} \cdot cm^{-2}$	[54]
	LIP	CO_2 laser	PI film + Ni + Au	Sensitivity: 3500 $\mu A \cdot mM^{-1} \cdot cm^{-2}$	[99]
	LIP	CO_2 laser	PI film + PEDOT	Sensitivity: (glucose) 3.87 $\mu A \cdot mM^{-1}$; (lactate) 11.83 $\mu A \cdot mM^{-1}$	[95]
	LIP	CO_2 laser	PI film + Cu NPs	Sensitivity: 495 $\mu A \cdot mM^{-1} \cdot cm^{-2}$	[97]
Gas sensor	LIP	CO_2 laser	PI film + MoS_2 casting	NO_2 gas: −47.6%; Response time: 2.87 min	[179]
	LIP	CO_2 laser	PI film + elastomeric materials + Ag coating	NO_2 gas: 5%; Response time: 360 s; Recovery time 720 s; LOD: 1.2 ppb	[92]
	LIP	CO_2 laser	PI film	NO_2 gas: 6.66‰ ppm^{-1}; LOD: 4 ppb NO gas: 4.18‰ ppm^{-1}; LOD: 8.3 ppb	[93]
	LIP	532 nm (CW)	Paper	NO_2 gas: 0.16% (40 ppm); LOD: 5 ppm	[38]
	LIG jetting	532 nm (CW)	PI film	NO_2 gas: 1‰ (5 ppm); LOD: 28 ppb	[128]
	Laser reduction	CO_2 laser	Graphene + MXene	NO_2/NH_3 gas: 1% ppm^{-1}; LOD: 5 ppb	[71]
Humidity sensor	LIP	CO_2 laser	PI film + GO drop casting	RH: 11%–97%	[90]
	LIP	CO_2 laser	LIG + ZIS	RH: 40%–90%	[103]

Table 3 (continued)

Application	Laser process	Laser source	Materials	Performance	Reference
	LIP	CO_2 laser	LIG + ZIS	RH: 30%–90%	[94]
	LIP	CO_2 laser	Pb/HNb_3O_8 stacked on LIG electrodes	RH: 30%–90%	[91]
	SLS	355 nm (ns)	Ga_2O_3 + LM on PI film	RH: 30%–95%	[158]
	Laser printing	800 nm fs laser	PEDOT:PSS	RH: 11%–69%	[180]
	Laser ablation	CO_2 laser	Cotton denim fabric + conductive textile	RH: 10%–90%	[132]
	Laser annealing	808 nm laser	Metal–oxide material (indium zinc oxide)	RH: 10%–60%	[166]

LIP: laser-induced pyrolysis; LIG: laser-induced graphene; SLS: selective laser sintering; CW: continuous-wave; PI: polyimide; PEDOT:PSS: poly(3,4-ethylenedioxythiophene):poly(styrene sulfonate); NP: nanoparticle; GO: graphene oxide; ZIS: $ZnIn_2S_4$; LM: liquid metal; LOD: limit of detection; RH: relative humidity. 1 M =1 mol/L; 1 ppm =1 $\times 10^{-6}$; 1 ppb =1 $\times 10^{-9}$

through the laser engraving of LIG and microfluidic channels [177] enabled the real-time detection of uric acid (UA) and tyrosine (Tyr) in sweat. The in-depth investigation of sweat UA and Tyr, which are important diagnostic indicators for the management of gout and other metabolic disorders [186, 187], is considered a major challenge because their levels are extremely low. Accelerated electron transfer [188] and catalytic activation in enhanced redox reactions [189] through the presence of abundant defects make LIG an ideal candidate for electrochemical biosensors. Supported by the fully integrated microfluidic chamber system, the continuous operation of contamination-free collection, supply of sweat at a constant rate, and chemical sensing are well exhibited. For vital sign monitoring, the strain-resistive LIG temperature sensor shows improved conductivity with an increasing temperature owing to the increased electron–phonon scattering speed and thermal velocity of electrons [28], and the 3D porous strain sensor simultaneously reads the external strain deformations. Thus, multistep all-laser processing endows wearable multimodal biosensors with efficient microfluidic system integration for accurate sensing under continuous sweat sampling and multimodal vital sign monitoring.

Furthermore, the hybrid processing of transformative laser-induced pyrolysis and conventional laser drilling may leverage each process for the fabrication of multifunctional bioelectronic devices [190]. As shown in Fig. 9a, programmable patterned LIG sensors are monolithically interconnected with functional hydrogel and highly conductive liquid metal electrodes, which constitute consecutive multilayers of electrical elements and substrates. On the attachment surface of the device, penetration holes are selectively made to directly expose the humidity sensor and electrocardiogram (ECG) sensor to the skin. The elastomeric characteristics of the hydrogel–PDMS hybrid layer are used for the deflection of cracks to prevent complete fracture during strain deformation (Fig. 9b) and conformal contact (Fig. 9c), whereas the LIG-based wearable sensing system can be successfully applied to the skin interface.

Another useful combination of sequential laser processes is the UV laser ablation of cPI for stretchable designs and the annealing of metal NPs by laser sintering for conductive electronic channel fabrication [155] (Fig. 9d). The 2D, thin, and serpentine-patterned skin-interfaced sensor produces initial cracks in the laser-annealed layer before being attached to the skin to activate the entire sensory system. When the sensor is attached to cover a wide area of the wrist, the relative resistance responses to epicentral deformation by the complex strain stress of the five fingers are decoded using a deep-learning algorithm to provide real-time human motion data (Fig. 9e). To fine-tune detection sensitivity, laser fluence can be used to modulate the porosity of the sintered NP structures by adjusting the degree of annealing; thus, the programmable crack propagation depth determines the gauge factor of the sensor (Fig. 9f). Therefore, minute skin deformations from epicentral reactions of remote body sites can be readily measured under low laser fluence conditions using a suitable laser-induced crack-based strain sensor as well as deep-learning technology. In summary, the multistep processing of all-laser fabrication methods reveals their potential as a facile alternative to inefficient procedures and substantiates their outstanding performance and biocompatibility for skin-interfaced wearable applications.

Multiple laser sources

Recently, researchers have introduced innovative technologies for wearable devices that involve the development and optimization of thin-film electronic components through the use of two lasers having different wavelengths [156]. The proposed technology is based on a dual-process approach called multilaser processing (Fig. 10a): (1) Additive manufacturing. This involves the laser sintering of metal NPs

Table 4 Physical sensors

Application	Laser process	Laser source	Materials	Performance	Reference
Strain sensor	LIP	CO_2 laser	PI film + ZnSe	GF: 107,428 (at −0.09%–0.09% strain)	[26]
	LIP	CO_2 laser	PI film + Co NPC	GF: 1177 (0%–18%), 39,548 (18%–23%)	[88]
	LIP	CO_2 laser	PI film + PDMS	GF: 37.8 (at 31.8% strain)	[18]
	LIP	CO_2 laser	PEEK	GF: 1.06 (0%–60%)	[56]
	LIP	CO_2 laser	PI film + PDMS	GF: 3.54 (at 0%–100% strain)	[23]
	LIP	CO_2 laser	PI film + Ecoflex with crack	GF: 114.8 (approximately 50% strain)	[15]
	LIP	CO_2 laser	PI film + PDMS	GF: 950 (at 20%–30% strain)	[16]
	LIP	355 nm ps laser	PI fabric	GF: 27 (at 4% strain)	[19]
	LIP	355 nm pulsed laser	PDMS + PSPI	GF: 21–35 (at 0%–1% strain)	[80]
	LIP	–	PDMS + PI particles	GF: Linear range (3%–79%), 59 (0%–3%), 606 (3%–7%), 1948 (>7%)	[81]
	Laser-induced graphitization	460 nm laser	Lignin paper	GF: (Tensile) 201 (strain: 0%–0.025%), 255 (0.025%–0.125%), 408 (0.125%–0.225%); (Compressive) 91 (0%–0.025%), 70 (0.125%–0.225%)	[50]
	LIP and SLS	CO_2 laser	PI film + PDMS	GF: 243.42 (0%–30%), 2710.95 (30%–40%)	[69]
	LDW	355 nm ps laser	PI film + Pt precursor + PDMS	GF: 45.6 (0%–6%), 269.5 (6%–17%), 489.3 (17%–20%)	[60]
	rGO	780 nm fs laser	GO + Ag	GF: 52.5 (<25.4% strain)	[32]
	Laser cutting	1060 nm pulsed laser	Ti_3C_2–MXene	GF: 7400 (at 0.7% strain)	[110]
	Laser engraving	UV laser marker	Carbon-added PDMS + Ag	GF: tunable from 3.4 to 4570.6	[119]
	Laser ablation	CO_2 laser	PDMS/MWCNT composite	GF: 513.2 (at 5% strain)	[113]
	Laser ablation and laser patterning	515 nm fs laser	PDMS + graphene	GF: 496.7	[115]
	Laser ablation and laser annealing	355 nm ns laser	Crack-induced Ag layer on cPI	GF: >2000	[155]
Pressure sensor	LIP	CO_2 laser	PI film + PU transfer	Sensitivity: 149 kPa^{-1} (0–1 kPa), 659 kPa^{-1} (1–10 kPa), 2048 kPa^{-1} (10–100 kPa)	[24]
	LIP	CO_2 laser	PI film + Ag NP on MX sponge	Sensitivity: 0.9 kPa^{-1} at 0.5 kPa	[104]
	LIP	CO_2 laser	PI film + LIG powder	Sensitivity: 1.86 kPa^{-1} at 0–150 Pa	[25]

Table 4 (continued)

Application	Laser process	Laser source	Materials	Performance	Reference
	LIP	CO_2 laser	MWCNTs + PDMS + PI film	Sensitivity: 2.41 kPa^{-1} at 0–200 Pa	[70]
	LIP	CO_2 laser	PI film + PDMS	Sensitivity: 8.5×10^{-3} kPa^{-1} at 0–30 kPa, 1.2×10^{-3} kPa^{-1} at 30–220 kPa	[23]
	LIP	CO_2 laser	PI film + Ecoflex with cracks	Sensitivity: 1.64×10^{-2} kPa^{-1} at 0–120 kPa	[15]
	LIG	CO_2 laser	PI film + GO cloth	Sensitivity: 30.3 kPa^{-1} at 0–2.5 kPa, 0.56 kPa^{-1} at 2.5–20 kPa	[87]
	LDW	915 nm laser	PI film	Sensitivity: Linear range at 0–100 kPa; Resolution: mPa scale	[14]
	rGO	CO_2 laser	GO + cellulose fiber	Sensitivity: 19.47 kPa^{-1} at 0–4 kPa	[49]
	LSG	450 nm laser	Graphene oxide	Sensitivity: 434 kPa^{-1} at 200 kPa	[33]
	Laser ablation	355 nm fs laser	PDMS + Ag NW coating	Sensitivity: 4.48 kPa^{-1} at 0–22 kPa	[122]
	Laser ablation	800 nm fs laser	PDMS + LM	Sensitivity: about 2.78 kPa^{-1}	[143]
Temperature sensor	LIP	532 nm (CW)	Paper	Temperature resistance coefficient, R(T): -0.15% $°C^{-1}$	[38]
	LIP	1064 nm pulsed laser	PI film	R(T): 0.00142 $°C^{-1}$ with high linearity ($R^2 = 0.999$)	[17]
	rGO	CO_2 laser	GO + cellulose fiber	R(T): -0.195% $°C^{-1}$ at 30–50 °C	[49]
	SLS	532 nm (CW)	Ni NP	(Heater): 310 °C at 11 V	[181]
	Laser welding	940 nm laser	Metal foil textile	R(T): 0.0039 $°C^{-1}$, R^2 of 0.997	[169]
	Laser ablation	355 nm ns laser	Thermoelectric pellet	(Thermo-haptic device): Cooling: 11 °C; Heating: 40 °C	[129]
	Laser curing and laser pattering	1064 nm pulsed laser	Si + Polymer	(Heater): 80 °C at 3 W/cm^2	[167]
	Laser-induced reductive sintering	532 nm (CW)	Ni–NiO–Ni	R(T): -9.2% $°C^{-1}$ (20–30 °C), B-value: 7350 K (25–70 °C), 8162 K (25–30 °C)	[157]
Optical sensor	LIP and SLS	CO_2 (CW) and 800 nm fs laser	ZnO NP on PI film	(Photodetector) Responsivity: 0.1–0.9 mA/W (2.4–3.1 W); Dual-mode (UV/IR)	[78]
	LIHG	532 nm (CW)	ZnO NW + CuO NW	(Photodetector) Responsivity: 2.39×10^{-4} A/W (bias: 2 V); Photocurrent density: 1.25 A/cm^2	[163]
	Laser-induced redox	532 nm (CW)	Cu	(Photodetector) Multispectral to RGB	[176]

Table 4 (continued)

Application	Laser process	Laser source	Materials	Performance	Reference
	Laser texturing	520 nm fs laser	AISI304 stainless steel	(SERS sensor) LOD: 10^{-14} M	[148]
	Laser drilling, laser ablation, and laser texturing	520 nm fs laser	–	(SERS sensor) LOD: 10^{-17} M	[149]
	Laser carbonization and graphitization	400–460 nm laser	Resorcinol–formaldehyde (RF) aerogel	(Photodetector) Sensitivity: 0.12% mW^{-1} at infrared light	[48]
	SiC sintering	800 nm fs laser	SiC NPs	(Photodetector) Responsivity: 55.89 A/W (bias: 1 V) under UV light	[164]
Sound sensor	LIP	CO_2 laser	PI film	Sound pressure level: 49 dB at 20 kHz	[182]
	Laser ablation	–	Kapton + PI + PVDF + Ag	Resonant frequency at 199.37 kHz	[121]
	LIP and laser engraving	CO_2 and 355 nm (ns)	LIG + PDMS	Peak acceleration: 6–68.5 m/s^2	[183]

LIP: laser-induced pyrolysis; SLS: selective laser sintering; LDW: laser direct writing; rGO: reduced graphene oxide; LIG: laser-induced graphene; LSG: laser-scribed graphene; LIHG: laser-induced hydrothermal growth; UV ultraviolet; CW: continuous-wave; PI polyimide; NPC: nanoparticle cluster; PDMS: polydimethylsiloxane; PEEK: polyether ether ketone; PSPI: photosensitive polyimide; GO: graphene oxide; MWCNT multiwalled carbon nanotube; cPI: colorless polyimide; PU: polyurethane; NP: nanoparticle; LM: liquid metal; NWs: nanowires; PVDF: polyvinylidene fluoride; GF: gauge factor; IR: infrared; LOD: limit of detection; SERS: surface-enhanced Raman spectroscopy

using visible wavelength. A continuous 532 nm laser selectively sinters Ag NPs coated onto a cPI film and forms a predetermined metal pattern that constitutes an electrically connected layer. (2) Cutting. Performed using UV laser ablation, this step selectively removes the top Ag NP electrode without damaging the substrate or the previously patterned bottom layer electrode. This is because materials absorb and transmit light differently depending on their wavelength. The high absorption rate of Ag NPs at 532 nm facilitates their sintering through a photothermal reaction, whereas the low-power 355 nm laser ablates the Ag NP electrodes without penetrating the layer or harming the substrate. The flexibility to create and erase electrodes with these multilasers enables the real-time modification of electrode patterns during fabrication. The resulting attachable wireless networking multimode wearable devices exhibit impedance optimization that depends on the operating frequency. Figure 10b illustrates the ability to adjust the impedance, which is critical for various attachment locations and users, in real time by modifying an antenna designed through the multilaser process. Moreover, researchers have successfully developed wireless wearable devices that operate without batteries by implementing radiofrequency (RF) energy harvesting through impedance optimization, which demonstrates their potential application in commercial equipment such as VR and skin devices (Fig. 10c).

A recent study introduced a fully soft, self-driven vibration sensor (SSVS) using a multilaser process for PDMS texturing and LIG patterning [183]. As shown in Fig. 10d, the SSVS was fabricated by combining PDMS and PI films using various techniques, including laser pyrolysis, laser engraving, and laser texturing. The SSVS manufacturing process is as follows. Initially, to capture electrical signals generated by the vibration of a Galinstan droplet, LIG electrodes were created on a PI film through a photothermal reaction using an infrared laser. The LIG electrodes were then transferred onto flexible and stretchable PDMS substrates. Subsequently, the LIG electrodes transferred onto the PDMS were textured using a low-thermal-effect UV-pulsed laser to create a nonwetting structure. In addition, a pulsed laser was employed on the PDMS cap to establish an engraved pattern to protect the Galinstan droplets. The nonwetting characteristics of PDMS cap were motivated by the characteristics of pulsed lasers, which do not carbonize LIG or PDMS, but rather ablate them. The LIG electrodes exhibited electrical insulation and high resistance due to the destruction caused by the high-energy intensity of the UV-pulsed laser. The texture of the PDMS influences the CA with the Galinstan droplets. These properties can be finely adjusted based on the laser parameters to enhance sensor functionality. With increasing laser fluence, the laser-textured notch in the LIG electrode deepens, which increases the specific surface area. This amplifies the signal due to the enhanced friction-charging efficiency of the Galinstan droplet. Moreover, precise control of the hatch size and laser fluence facilitates the creation of dense, deeply textured surfaces, thereby aiding the Galinstan droplet to keep a stable shape while retaining a large CA. By sensing subtle vibrations through a stabilized Galinstan droplet, the SSVS can be

Table 5 Energy storage devices

Application	Laser process	Laser source	Materials	Performance	Reference
Triboelectric nanogenerators	LIP	CO_2 laser	PI film	Power density: 512 mW/m^2	[13]
	LIP	CO_2 laser	PI film + PTFE coating/GO-Cu coating	Power density: 41 $\mu W/cm^2$	[86]
	LIP	CO_2 laser	PEEK	Power density: 2.3 mW/cm^2	[56]
	LIP	CO_2 laser	PI film + rGO cloth	Transfer charge density: 270 $\mu C/m^2$	[87]
	Laser ablation	CO_2 laser	FPCB	Power density: 416 mW/m^2	[184]
	Laser ablation	355 nm pulsed laser	PI film + SRPA + Al	Power density: 98.35 mW/m^2	[120]
	Laser synthesis	1064 nm pulsed laser	Si + MoS_2	Power: 2.25 μW	[34]
	Laser reduction	CO_2 laser	Graphene/MXene	Power density: 57 mW/cm^2	[71]
Thermoelectric generator	Laser ablation	1064 nm pulsed laser	Thermoelectric film	Power density: 1.04 mW/cm^2	[117]
	Laser engraving	CO_2 laser	Ag + Ti + PDMS films	Power: 7.9 μW	[131]
Moisture-driven power generator	LIP	CO_2 laser	Cellulose nanofiber	Power density: 4.92 $\mu W/m^2$	[46]
Supercapacitor	LIP	CO_2 laser	PI film + Co_3O_4 precursor	Capacitance: 10.9 mF/cm^2 at 5 mV/s; PVA/H_2SO_4	[61]
	LIP	CO_2 laser	PI film + KOH	Capacitance: 244 $\mu F/cm^2$ at 100 mV/s; PVA/H^+	[57]
	LIP	CO_2 laser	PI film + KOH	Capacitance: 32 mF/cm^2 at 20 mV/s; PVA/H_3PO_4	[58]
	LIP	450 nm laser	PI film	Capacitance: 8.11 mF/cm^2 at 100 mV/s; PVA/H_2SO_4	[27]
	LIP	CO_2 laser	Carbon cloth + MoO_2	Capacitance: 81.8 mF/cm^2 at 10 mV/s; Mo ion ink	[62]
	LIP	CO_2 laser	PAA film + MoS_2	Capacitance: 35.3 mF/cm^2 at 5 mV/s; PVA/NaOH	[59]
	LIP	CO_2 laser	PI film + PTFE + phosphorus copper sheets	Capacitance: 389.6 $\mu F/cm^2$ at 10 mV/s; PVA/Na_2SO_4	[84]
	LIP	346 nm fs laser	Leaf	Capacitance: 34.68 mF/cm^2 at 5 mV/s; PVA/H_2SO_4	[43]
	LIP	1064 nm laser	Cork	Capacitance: 1.35 mF/cm^2 at 5 mV/s; PVA/H_2SO_4	[39]
	LIP	450 nm laser	Paper	Capacitance: 166.6 mF/cm^2 at 50 mV/s; H_2SO_4	[82]
	LIP	532 nm fs laser	Lignin	Capacitance: 0.19 mF/cm^2 at 1500 mV/s; NaCl	[40]
	LIP	450 nm laser	Lignin-based fiber membranes + MoS_2	Capacitance: 527.8 F/g at 10 mV/s; PVA/H_2SO_4	[51]
	LIP	CO_2 laser	Kevlar textile	Capacitance: 125.35 mF/cm^2 at 100 mV/s; PVA/H_2SO_4	[53]
	LIP	532 nm laser	PI film	Capacitance: 1.59 mF/cm^2 at 100 mV/s; Na_2SO_4	[128]

Table 5 (continued)

Application	Laser process	Laser source	Materials	Performance	Reference
	LIP + synthesis	CO_2 laser	PI film + Ni/Co ion ink/WPU transfer	Capacitance: 2.4 mF/cm^2 at 10 mV/s; PVA	[67]
	LIP + synthesis	532 nm pulsed laser	PEEK + MnO_2 coating	Capacitance: 48.9 mF/cm^2 at 10 mV/s; PVA/H_2SO_4	[55]
	SLS	355 nm pulsed laser	SWCNTs/MWCNTs + rGO/Ag NWs	Capacitance: 4 F/cm^2 at 5 mV/s; PVA/H_3PO_4	[152]
	SLS	532 nm laser	PVDF + Ag NPs	Capacitance: 24.5 mF/cm^2 at 50 mV/s; PVA/Na_2SO_4	[153]
	Laser scribing	CO_2 laser	PI film + PEDOT	Capacitance: 115.2 F/g at 10 mV/s; Aqueous electrolyte	[83]
	Laser reduction	1030 nm fs laser	GO + PDMS	Capacitance: 52 F/cm^3 at 5 mV/s; PVA/H_2SO_4	[29]
	Laser deposition	KrF excimer laser	V_2O_5 and WO_3 thin films	Capacitance: 40.28 F/cm^3 at 500 mV/s; PVA/KOH	[185]
	Laser engraving	CO_2 laser	PI film + MnO_2	Capacitance: 15.04 mF/cm^2 at 5 mV/s; PVA/KOH	[68]
	LDW	UV laser	$Ti_3C_2T_x$ MXene	Capacitance: 241 mF/cm^2 at 100 mV/s; PVA/H_2SO_4	[111]
	Laser ablation	1064 nm laser	PEDOT:PSS-aramid nanofiber	Capacitance: 15.4 mF/cm^2 at 2 mV/s; PVA/H_3PO_4	[112]
Fuel cells	LIP + ablation	450 nm laser	Paper	Power density: 27 μW/cm^2	[82]
	Laser scribing	CO_2 laser	PI film/glucose dehydrogenase + bilirubin oxidase	Power density: (27±1.7) μW/cm^2	[85]
Battery	LIP + SLS	CO_2 laser	PI film + Co_3O_4 precursor	Capacitance: 712 mAh/g	[69]
	Laser engraving	CO_2 laser	MWCNT-MnO_2 or MWCNT-Zn	Capacitance: 116.6 μAh/cm^2	[114]
	Laser ablation	1064 nm ps laser	$LiFePO_4$/$Li_4Ti_5O_{12}$ powders	Capacitance: 1.2 mAh/cm^2	[118]

LIP: laser-induced pyrolysis; SLS: selective laser sintering; LDW: laser direct writing; rGO: reduced graphene oxide; LIG: laser-induced graphene; UV: ultraviolet; PI: polyimide; PDMS: polydimethylsiloxane; PEEK polyether ether ketone; GO: graphene oxide; MWCNT: multiwalled carbon nanotube; NP: nanoparticle; NW: nanowires; PVDF: polyvinylidene fluoride; WPU: waterborne polyurethane; PAA: polyacrylic acid; SRPA: silicon rubber polyamide; FPCB: flexible printed circuit board; PTFE: polytetrafluoroethylene; SWCNT: single wall carbon nanotube; PVA: polyvinyl acetate

integrated with a Bluetooth module. This integration enables the detection of human movement via applications that monitor subtle liquid vibrations in real time. This system is further equipped with the functionality to identify emergencies, such as falls and slips (Fig. 10e).

Conclusions

In this review, selective laser processes that apply to the fabrication of wearable devices are classified and summarized to assess the status of relevant technologies. For the transformative approach represented by LIG, in-depth studies have been conducted in terms of design optimization and material selection. The use of additional materials enables the rapid generation of more complex, hierarchical nanostructures that provide enhanced performance or additional functionality to a device. In conventional laser processing, such as micromachining, sintering, and synthesis, notable improvements have been achieved via the expansion of applicable materials from metal to nanomaterials, polymers, and native materials, smart modifications to the existing method, and the discovery of novel applications enabled by the corresponding schemes. These laser processes function as core fabrication methods for individual elements that are vital for wearable applications, including human motion detection, energy harvesting, sweat sensors, and real-time health monitoring. As the use of lasers for the fabrication of wearable devices continues to

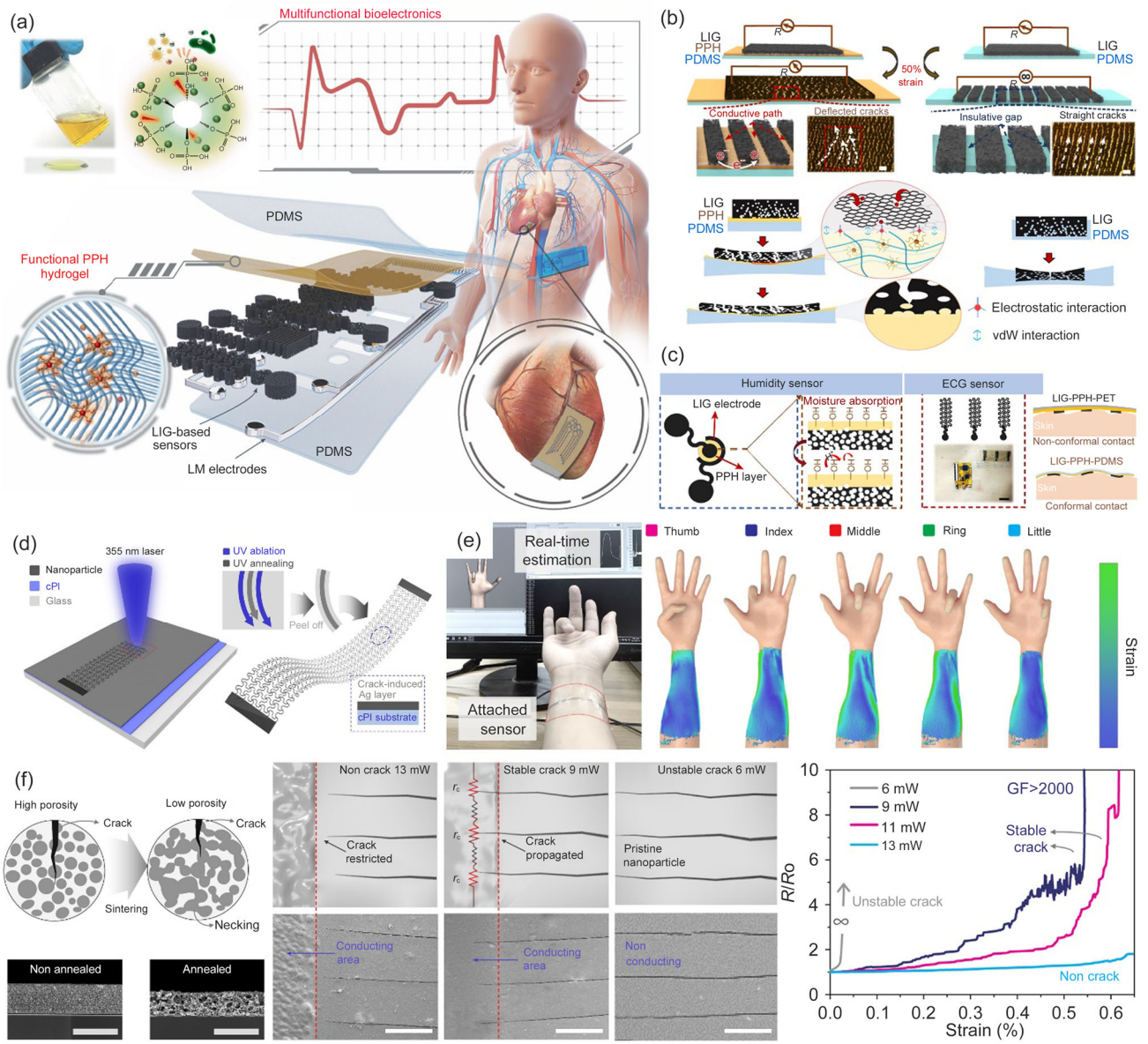

Fig. 9 **a** Illustration of a wearable and implantable bioelectronic device fabricated with multistep laser processing. **b** Schematic of the difference in crack propagation characteristics with (left) and without (right) a polyvinyl acetate–phytic acid–honey (PPH) interlayer. **c** Bioelectronic sensing applications of the laser-induced graphene (LIG)-based wearable sensor. Reproduced from Ref. [190], Copyright 2023, with permission from the authors, under exclusive license to Springer Nature Limited. **d** Schematic of multistep laser processing. **e** Real-time estimation of human finger motion by detection of varying strains. **f** Programmable crack propagation depth by controlled laser fluence parameters and the resultant sensitivity of the laser-induced crack-based strain sensor. Reproduced from Ref. [155], Copyright 2020, with permission from the authors, licensed under CC BY 4.0

increase, we expect that a selective laser process will become indispensable to the ambient manufacturing of multifunctional wearable devices.

Future development directions in laser processing can be anticipated based on the latest wearable devices mentioned in Sect. "Applications." We first observe that recent studies on wearable devices not only demonstrate the proof-of-concept functionalities of individual components but also progress toward integration at the system level, which is much more challenging. For instance, for the standalone operation of wearable sensor devices at the system level, data acquired from a sensor must be processed and transmitted, which requires several additional components in addition to a sensing element, such as a microcontroller or converter [177]. Consequently, the compatibility of the laser process with

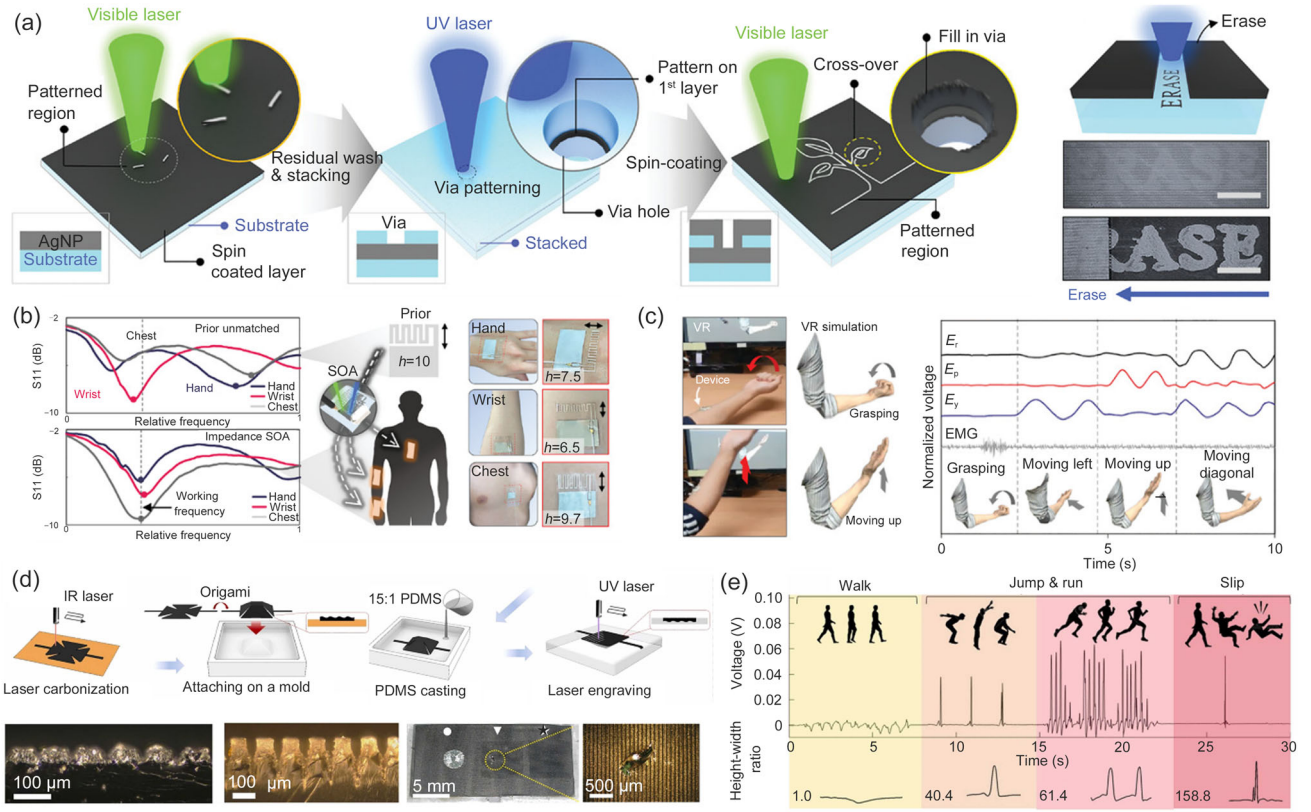

Fig. 10 **a** Schematic of the laser sintering and ablation processes using multiple lasers. **b** Different impedance optimization depending on skin attachment location. **c** Motion detection testing with wireless wearable sensors. Reproduced from Ref. [156], Copyright 2021, with permission from Wiley–VCH GmbH. **d** Top: schematic for the fabrication of a self-driven vibration sensor (SSVS); bottom: images of laser-induced graphene/polydimethylsiloxane (LIG/PDMS) according to laser texturing. **e** Contextual motion detection graph using SSVS. Reproduced from Ref. [183], Copyright 2022, with permission from Elsevier

other fabrication techniques and the intimate electrical contact between distinct elements created by different processes should be considered. More than two laser processes were employed in the selected studies, which suggest that the all-laser-fabricated wearable device is a desirable concept.

However, the full potential of laser processing has not yet been realized. Currently, laser processes used in the production of wearable devices largely rely on accessible lasers without detailed investigations of laser conditions for fabrication optimization, such as wavelength, pulse width, and repetition rate. However, the characteristics, and hence the performance of the resultant device, vary significantly depending on the laser conditions, even for a given material [191–193]. Thus, we expect research institutions specializing in lasers to be more actively involved in relevant projects of all-laser processes. Experts in high-power lasers are also needed for solving the persistent problem of low throughput in laser processes. Through these research activities, we expect that the development of laser processes for wearable devices and their production will undergo significant evolution.

Acknowledgements This work was supported by the Basic Research Program through the National Research Foundation of Korea (NRF) (Nos. 2022R1C1C1006593, 2022R1A4A3031263, and RS-2023-00271166), the National Science Foundation (Nos. 2054098 and 2213693), the National Natural Science Foundation of China (No. 52105593), and Zhejiang Provincial Natural Science Foundation of China (No. LDQ24E050001). EH acknowledges a fellowship from the Hyundai Motor Chung Mong-Koo Foundation.

Author contributions SH and HP conceived and designed the work. YK, EH, and SH investigated the literature and prepared scientific figures. YK, EH, CK, HP, and SH wrote original draft. YK, EH, and SH revised the manuscript. KCX provided valuable discussions. KCX, HP, and SH applied for funds. HP and SH supervised the overall work. All authors have read and approved this manuscript for publication.

Data availability statement Research data are not shared.

Declarations

Conflict of interest This paper is to be included in a special issue for which KCX is a guest editor. KCX is also an academic editor for *Bio-Design and Manufacturing*. He was not involved in the editorial review or the decision to publish this article. The authors declare that they have no conflict of interest.

Ethical approval This study does not contain any studies with human or animal subjects performed by any of the authors.

References

1. Truong PL, Yin Y, Lee D et al (2023) Advancement in COVID-19 detection using nanomaterial-based biosensors. Exploration 3(1):20210232. https://doi.org/10.1002/EXP.20210232
2. Yeo J, Hong S, Lee D et al (2012) Next generation non-vacuum, maskless, low temperature nanoparticle ink laser digital direct metal patterning for a large area flexible electronics. PLoS ONE 7(8):e42315. https://doi.org/10.1371/journal.pone.0042315
3. Kim DC, Shim HJ, Lee W et al (2020) Material-based approaches for the fabrication of stretchable electronics. Adv Mater 32(15):e1902743. https://doi.org/10.1002/adma.201902743
4. Xue ZG, Song HL, Rogers JA et al (2020) Mechanically-guided structural designs in stretchable inorganic electronics. Adv Mater 32(15):e1902254. https://doi.org/10.1002/adma.201902254
5. Son Y, Yeo J, Moon H et al (2011) Nanoscale electronics: digital fabrication by direct femtosecond laser processing of metal nanoparticles. Adv Mater 23(28):3176–3181. https://doi.org/10.1002/adma.201100717
6. O'Halloran S, Pandit A, Heise A et al (2023) Two-photon polymerization: fundamentals, materials, and chemical modification strategies. Adv Sci 10(7):e2204072. https://doi.org/10.1002/advs.202204072
7. Bäuerle D (2011) Laser Processing and Chemistry. Springer, Berlin, Germany. https://doi.org/10.1007/978-3-642-17613-5
8. Qu ZH, Sun SF, Wang J et al (2023) Application of ultrafast laser beam shaping in micro-optical elements. J Laser Appl 35(3):24. https://doi.org/10.2351/7.0001033
9. Grigoropoulos CP (2009) Transport in Laser Microfabrication. Cambridge University Press, UK. https://doi.org/10.1017/CBO9780511596674
10. Park H, Park JJ, Bui PD et al (2023) Laser-based selective material processing for next-generation additive manufacturing. Adv Mater 2023:e2307586. https://doi.org/10.1002/adma.202307586
11. Hong S, Lee H, Yeo J et al (2016) Digital selective laser methods for nanomaterials: from synthesis to processing. Nano Today 11(5):547–564. https://doi.org/10.1016/j.nantod.2016.08.007
12. Lin J, Peng ZW, Liu YY et al (2014) Laser-induced porous graphene films from commercial polymers. Nat Commun 5:5714. https://doi.org/10.1038/ncomms6714
13. Choi KH, Park S, Hyeong SK et al (2020) Triboelectric effect of surface morphology controlled laser induced graphene. J Mater Chem A 8(38):19822–19832. https://doi.org/10.1039/d0ta05806h
14. Chen L, Hu B, Gao X et al (2022) Double-layered laser induced graphene (LIG) porous composites with interlocked wave-shaped array for large linearity range and highly pressure-resolution sensor. Compos Sci Technol 230:109790. https://doi.org/10.1016/j.compscitech.2022.109790
15. Wei S, Liu YJ, Yang LN et al (2022) Flexible large e-skin array based on patterned laser-induced graphene for tactile perception. Sens Actuat A Phys 334:113308. https://doi.org/10.1016/j.sna.2021.113308
16. Huang YX, Tao LQ, Yu JB et al (2020) Integrated sensing and warning multifunctional devices based on the combined mechanical and thermal effect of porous graphene. ACS Appl Mater Interfaces 12(47):53049–53057. https://doi.org/10.1021/acsami.0c13909
17. Gandla S, Naqi M, Lee M et al (2020) Highly linear and stable flexible temperature sensors based on laser-induced carbonization of polyimide substrates for personal mobile monitoring. Adv Mater Technol 5(7):2000014. https://doi.org/10.1002/admt.202000014
18. Huang LX, Wang H, Wu PX et al (2020) Wearable flexible strain sensor based on three-dimensional wavy laser-induced graphene and silicone rubber. Sensors 20(15):4266. https://doi.org/10.3390/s20154266
19. Liu W, Huang YH, Peng YD et al (2020) Stable wearable strain sensors on textiles by direct laser writing of graphene. ACS Appl Nano Mater 3(1):283–293. https://doi.org/10.1021/acsanm.9b01937
20. He MH, Wang YN, Wang SR et al (2020) Laser-induced graphene enabled 1D fiber electronics. Carbon 168:308–318. https://doi.org/10.1016/j.carbon.2020.06.084
21. Han S, Hong S, Ham J et al (2014) Fast plasmonic laser nanowelding for a Cu-nanowire percolation network for flexible transparent conductors and stretchable electronics. Adv Mater 26(33):5808–5814. https://doi.org/10.1002/adma.201400474
22. Li YL, Luong DX, Zhang JB et al (2017) Laser-induced graphene in controlled atmospheres: from superhydrophilic to superhydrophobic surfaces. Adv Mater 29(27):8. https://doi.org/10.1002/adma.201700496
23. Raza T, Tufail MK, Ali A et al (2022) Wearable and flexible multifunctional sensor based on laser-induced graphene for the sports monitoring system. ACS Appl Mater Interfaces 14(48):54170–54181. https://doi.org/10.1021/acsami.2c14847
24. Tian Q, Yan WR, Li YQ et al (2020) Bean pod-inspired ultrasensitive and self-healing pressure sensor based on laser-induced graphene and polystyrene microsphere sandwiched structure. ACS Appl Mater Interfaces 12(8):9710–9717. https://doi.org/10.1021/acsami.9b18873
25. Zhao J, Gui JH, Luo JS et al (2021) Highly responsive screen-printed asymmetric pressure sensor based on laser-induced graphene. J Micromechan Microeng 32(1):9. https://doi.org/10.1088/1361-6439/ac388d
26. Yao YB, Jiang ZF, Yao JW et al (2020) Self-sealing carbon patterns by one-step direct laser writing and their use in multifunctional wearable sensors. ACS Appl Mater Interfaces 12(45):50600–50609. https://doi.org/10.1021/acsami.0c14949
27. Huang F, Feng GY, Yin JJ et al (2020) Direct laser writing of transparent polyimide film for supercapacitor. Nanomaterials 10(12):2547. https://doi.org/10.3390/nano10122547
28. Shao Q, Liu G, Teweldebrhan D et al (2008) High-temperature quenching of electrical resistance in graphene interconnects. Appl Phys Lett 92(20):202108. https://doi.org/10.1063/1.2927371
29. Lee YA, Lim J, Cho Y et al (2020) Attachable micropseudocapacitors using highly swollen laser-induced-graphene electrodes. Chem Eng J 386:123972. https://doi.org/10.1016/j.cej.2019.123972
30. Rodriguez RD, Khalelov A, Postnikov PS et al (2020) Beyond graphene oxide: laser engineering functionalized graphene for flexible electronics. Mater Horiz 7(4):1030–1041. https://doi.org/10.1039/c9mh01950b
31. Wei YH, Li XS, Wang YF et al (2021) Graphene-based multifunctional textile for sensing and actuating. ACS Nano 15(11):17738–17747. https://doi.org/10.1021/acsnano.1c05701
32. Wan ZF, Wang SJ, Haylock B et al (2021) Localized surface plasmon enhanced laser reduction of graphene oxide for wearable strain sensor. Adv Mater Technol 6(5):11. https://doi.org/10.1002/admt.202001191
33. Wu Q, Qiao YC, Guo R et al (2020) Triode-mimicking graphene pressure sensor with positive resistance variation for physiology and motion monitoring. ACS Nano 14(8):10104–10114. https://doi.org/10.1021/acsnano.0c03294

34. Park S, Park J, Kim Y et al (2020) Laser-directed synthesis of strain-induced crumpled MoS_2 structure for enhanced triboelectrification toward haptic sensors. Nano Energy 78:105266. https://doi.org/10.1016/j.nanoen.2020.105266
35. Zhang KM, Zhang JH, Liu YT et al (2021) A NIR laser induced self-healing PDMS/gold nanoparticles conductive elastomer for wearable sensor. J Colloid Interface Sci 599:360–369. https://doi.org/10.1016/j.jcis.2021.04.117
36. Nova NN, Zarzar LD (2022) Direct laser writing of graphitic carbon from liquid precursors. Chem Mater 34(10):4602–4612. https://doi.org/10.1021/acs.chemmater.2c00467
37. Zhao GG, Ling Y, Su YJ et al (2022) Laser-scribed conductive, photoactive transition metal oxide on soft elastomers for Janus on-skin electronics and soft actuators. Sci Adv 8(25):eabp9734. https://doi.org/10.1126/sciadv.abp9734
38. Jung Y, Min J, Choi J et al (2022) Smart paper electronics by laser-induced graphene for biodegradable real-time food spoilage monitoring. Appl Mater Today 29:1010589. https://doi.org/10.1016/j.apmt.2022.101589
39. Silvestre SL, Pinheiro T, Marques AC et al (2022) Cork derived laser-induced graphene for sustainable green electronics. Flex Print Electron 7(3):35021. https://doi.org/10.1088/2058-8585/ac8e7b
40. Miyakoshi R, Hayashi S, Terakawa M (2023) Direct patterning of conductive structures on hydrogels by laser-based graphitization for supercapacitor fabrication. Adv Electron Mater 9(5):2201277. https://doi.org/10.1002/aelm.202201277
41. Wang WT, Lu LS, Zhang DK et al (2023) Experimental and modeling study of laser induced silicon carbide/graphene on cotton cloth for superhydrophobic applications. Opt Laser Technol 158:108782. https://doi.org/10.1016/j.optlastec.2022.108782
42. Li ZH, Lu LS, Xie YX et al (2021) Preparation of laser-induced graphene fabric from silk and its application examples for flexible sensor. Adv Eng Mater 23(9):2100195. https://doi.org/10.1002/adem.202100195
43. Le TSD, Lee YA, Nam HK et al (2021) Green flexible graphene–inorganic-hybrid micro-supercapacitors made of fallen leaves enabled by ultrafast laser pulses. Adv Funct Mater 32(20):2107768. https://doi.org/10.1002/adfm.202107768
44. d'Amora M, Lamberti A, Fontana M et al (2020) Toxicity assessment of laser-induced graphene by zebrafish during development. J Phys Mater 3(3):34008. https://doi.org/10.1088/2515-7639/ab9522
45. Pinheiro T, Correia R, Morais M et al (2022) Water peel-off transfer of electronically enhanced, paper-based laser-induced graphene for wearable electronics. ACS Nano 16(12):20633–20646. https://doi.org/10.1021/acsnano.2c07596
46. Lee S, Eun J, Jeon S (2020) Facile fabrication of a highly efficient moisture-driven power generator using laser-induced graphitization under ambient conditions. Nano Energy 68:104364. https://doi.org/10.1016/j.nanoen.2019.104364
47. Lee CW, Jeong SY, Kwon YW et al (2022) Fabrication of laser-induced graphene-based multifunctional sensing platform for sweat ion and human motion monitoring. Sens Actuat A Phys 334:113320. https://doi.org/10.1016/j.sna.2021.113320
48. Ji XJ, Zhong Y, Li CY et al (2021) Nanoporous carbon aerogels for laser-printed wearable sensors. ACS Appl Nano Mater 4(7):6796–6804. https://doi.org/10.1021/acsanm.1c00858
49. Zhang HQ, He RY, Liu H et al (2021) A fully integrated wearable electronic device with breathable and washable properties for long-term health monitoring. Sens Actuat A Phys 322:112611. https://doi.org/10.1016/j.sna.2021.112611
50. Shen L, Zhou SK, Gu BS et al (2023) Highly sensitive strain sensor fabricated by direct laser writing on lignin paper with strain engineering. Adv Eng Mater 25(14):2201882. https://doi.org/10.1002/adem.202201882
51. Huang F, Zhou SK, Yan ZY et al (2023) Laser carbonization of lignin-based fiber membranes with heating treatment for flexible supercapacitors. Appl Surf Sci 619:156757. https://doi.org/10.1016/j.apsusc.2023.156757
52. Parmeggiani M, Stassi S, Fontana M et al (2021) Laser-induced graphenization of textile yarn for wearable electronics application. Smart Mater Struct 30(10):105007. https://doi.org/10.1088/1361-665X/ac182c
53. Rao YF, Yuan M, Gao B et al (2023) Laser-scribed phosphorus-doped graphene derived from Kevlar textile for enhanced wearable micro-supercapacitor. J Colloid Interface Sci 630(Pt A):586–594. https://doi.org/10.1016/j.jcis.2022.10.024
54. Mamleyev ER, Weidler PG, Nefedov A et al (2021) Nano- and microstructured copper/copper oxide composites on laser-induced carbon for enzyme-free glucose sensors. ACS Appl Nano Mater 4(12):13747–13760. https://doi.org/10.1021/acsanm.1c03149
55. Zhu CG, Dong X, Mei XS et al (2020) Direct laser writing of MnO_2 decorated graphene as flexible supercapacitor electrodes. J Mater Sci 55(36):17108–17119. https://doi.org/10.1007/s10853-020-05212-2
56. Li QS, Wu TY, Zhao W et al (2022) 3D printing stretchable core-shell laser scribed graphene conductive network for self-powered wearable devices. Compos Part B Eng 240:110000. https://doi.org/10.1016/j.compositesb.2022.110000
57. Bai SG, Tang Y, Wu YP et al (2020) High voltage microsupercapacitors fabricated and assembled by laser carving. ACS Appl Mater Interfaces 12(40):45541–45548. https://doi.org/10.1021/acsami.0c11935
58. Liu HL, Xie YX, Liu JB et al (2020) Laser-induced and KOH-activated 3D graphene: a flexible activated electrode fabricated via direct laser writing for in-plane micro-supercapacitors. Chem Eng J 393:124672. https://doi.org/10.1016/j.cej.2020.124672
59. Zhao J, Gao LJ, Wang ZT et al (2021) Boosting the performance of flexible in-plane micro-supercapacitors by engineering MoS_2 nanoparticles embedded in laser-induced graphene. J Alloy Compd 887:161514. https://doi.org/10.1016/j.jallcom.2021.161514
60. Liu W, Chen Q, Huang YH et al (2022) In situ laser synthesis of Pt nanoparticles embedded in graphene films for wearable strain sensors with ultra-high sensitivity and stability. Carbon 190:245–254. https://doi.org/10.1016/j.carbon.2022.01.020
61. Xu RQ, Liu P, Ji GH et al (2020) Versatile strategy to design flexible planar-integrated microsupercapacitors based on Co_3O_4-decorated laser-induced graphene. ACS Appl Energy Mater 3(11):10676–10684. https://doi.org/10.1021/acsaem.0c01744
62. Lin N, Chen HN, Wang WT et al (2021) Laser-induced graphene/MoO_2 core-shell electrodes on carbon cloth for integrated, high-voltage, and in-planar microsupercapacitors. Adv Mater Technol 6(5):200091. https://doi.org/10.1002/admt.202000991
63. Yi N, Cheng Z, Li H et al (2020) Stretchable, ultrasensitive, and low-temperature NO_2 sensors based on MoS_2@rGO nanocomposites. Mater Today Phys 15:100265. https://doi.org/10.1016/j.mtphys.2020.100265
64. Han X, Ye RQ, Chyan Y et al (2018) Laser-induced graphene from wood impregnated with metal salts and use in electrocatalysis. ACS Appl Nano Mater 1(9):5053–5061. https://doi.org/10.1021/acsanm.8b01163
65. Ye RQ, James DK, Tour JM (2018) Laser-induced graphene. Acc Chem Res 51(7):1609–1620. https://doi.org/10.1021/acs.accounts.8b00084
66. Tang Q, Zhou Z (2013) Graphene-analogous low-dimensional materials. Prog Mater Sci 58(8):1244–1315. https://doi.org/10.1016/j.pmatsci.2013.04.003

67. Wang WT, Lu LS, Xie YX et al (2020) A highly stretchable microsupercapacitor using laser-induced graphene/NiO/Co_3O_4 electrodes on a biodegradable waterborne polyurethane substrate. Adv Mater Technol 5(2):1900903. https://doi.org/10.1002/admt.201900903
68. Xu RQ, Wang ZT, Gao LJ et al (2022) Effective design of MnO_2 nanoparticles embedded in laser-induced graphene as shape-controllable electrodes for flexible planar microsupercapacitors. Appl Surf Sci 571:151385. https://doi.org/10.1016/j.apsusc.2021.151385
69. Chen X, Hou ZR, Li GX et al (2022) A laser-scribed wearable strain sensing system powered by an integrated rechargeable thin-film zinc-air battery for a long-time continuous healthcare monitoring. Nano Energy 101:107606. https://doi.org/10.1016/j.nanoen.2022.107606
70. Zhao J, Luo JS, Zhou ZW et al (2021) Novel multi-walled carbon nanotubes-embedded laser-induced graphene in crosslinked architecture for highly responsive asymmetric pressure sensor. Sens Actuat A Phys 323:112658. https://doi.org/10.1016/j.sna.2021.112658
71. Zhang C, Chen JG, Gao JD et al (2023) Laser processing of crumpled porous graphene/MXene nanocomposites for a standalone gas sensing system. Nano Lett 23(8):3435–3443. https://doi.org/10.1021/acs.nanolett.3c00454
72. Rethfeld B, Ivanov DS, Garcia ME et al (2017) Modelling ultrafast laser ablation. J Phys D Appl Phys 50(19):193001. https://doi.org/10.1088/1361-6463/50/19/193001
73. Jiang L, Tsai HL (2005) Energy transport and material removal in wide bandgap materials by a femtosecond laser pulse. Int J Heat Mass Transfer 48(3–4):487–499. https://doi.org/10.1016/j.ijheatmasstransfer.2004.09.016
74. Guo H, Qiao M, Yan JF et al (2023) Fabrication of hybrid supercapacitor by $MoCl_5$ precursor-assisted carbonization with ultrafast laser for improved capacitance performance. Adv Funct Mater 33(23):2213514. https://doi.org/10.1002/adfm.202213514
75. Pustovalov VK (2016) Light-to-heat conversion and heating of single nanoparticles, their assemblies, and the surrounding medium under laser pulses. RSC Adv 6(84):81266–81289. https://doi.org/10.1039/c6ra11130k
76. Jago R, Malic E, Wendler F (2019) Microscopic origin of the bolometric effect in graphene. Phys Rev B 99(3):035419. https://doi.org/10.1103/PhysRevB.99.035419
77. An JN, Le TSD, Lim CHJ et al (2018) Single-step selective laser writing of flexible photodetectors for wearable optoelectronics. Adv Sci 5(8):1800496. https://doi.org/10.1002/advs.201800496
78. Deng SF, Guo H, Yan JF et al (2023) NIR-UV dual-mode photodetector with the assistance of machine-learning fabricated by hybrid laser processing. Chem Eng J 472:144908. https://doi.org/10.1016/j.cej.2023.144908
79. McDonald JC, Duffy DC, Anderson JR et al (2000) Fabrication of microfluidic systems in poly(dimethylsiloxane). Electrophoresis 21(1):27–40. https://doi.org/10.1002/(SICI)1522-2683(20000101)21:1%3c27::AID-ELPS27%3e3.0.CO;2-C
80. Jeong SY, Lee JU, Hong SM et al (2021) Highly skin-conformal laser-induced graphene-based human motion monitoring sensor. Nanomaterials 11(4):951. https://doi.org/10.3390/nano11040951
81. Wang H, Zhao ZF, Liu PP et al (2021) Laser-induced porous graphene on polyimide/PDMS composites and its kirigami-inspired strain sensor. Theor Appl Mech Lett 11(2):100204. https://doi.org/10.1016/j.taml.2021.100240
82. Awasthi H, Jayapiriya US, Renuka H et al (2023) Flexible paper and cloth substrates with conductive laser induced graphene traces for electroanalytical sensing, energy harvesting and supercapacitor applications. IEEE Sens J 23(20):24078–24085. https://doi.org/10.1109/jsen.2022.3170538
83. Cho EC, Chang-Jian CW, Syu WL et al (2020) PEDOT-modified laser-scribed graphene films as bginder– and metallic current collector–free electrodes for large-sized supercapacitors. Appl Surf Sci 518:146193. https://doi.org/10.1016/j.apsusc.2020.146193
84. Bai SG, Tang Y, Chen G et al (2021) Phosphor copper-based flexible high voltage supercapacitors fabricated via laser irradiation and three-dimensional packaging. J Power Sources 507:230257. https://doi.org/10.1016/j.jpowsour.2021.230257
85. Kong X, Gai P, Ge L et al (2020) Laser-scribed N-doped graphene for integrated flexible enzymatic biofuel cells. ACS Sustain Chem Eng 8(33):12437–12442. https://doi.org/10.1021/acssuschemeng.0c03051
86. Kalasin S, Sangnuang P, Surareungchai W (2021) Wearable triboelectric sensors with self-powered energy: multifunctional laser-engraved electrets to activate satellite communication for life-emergency alert in pandemics. ACS Appl Electron Mater 3(12):5383–5392. https://doi.org/10.1021/acsaelm.1c00865
87. Xia SY, Long YF, Huang ZY et al (2022) Laser-induced graphene (LIG)-based pressure sensor and triboelectric nanogenerator towards high-performance self-powered measurement-control combined system. Nano Energy 96:107099. https://doi.org/10.1016/j.nanoen.2022.107099
88. Kim D, Chhetry A, Zahed MA et al (2023) Highly sensitive and reliable piezoresistive strain sensor based on cobalt nanoporous carbon-incorporated laser-induced graphene for smart healthcare wearables. ACS Appl Mater Interfaces 15(1):1475–1485. https://doi.org/10.1021/acsami.2c15500
89. Xu KC, Lu YY, Honda S et al (2019) Highly stable kirigami-structured stretchable strain sensors for perdurable wearable electronics. J Mater Chem C 7(31):9609–9617. https://doi.org/10.1039/c9tc01874c
90. Zhu CC, Tao LQ, Wang Y et al (2020) Graphene oxide humidity sensor with laser-induced graphene porous electrodes. Sens Actuat B Chem 325:128790. https://doi.org/10.1016/j.snb.2020.128790
91. Lu YY, Xu KC, Yang MQ et al (2021) Highly stable Pd/HNb_3O_8-based flexible humidity sensor for perdurable wireless wearable applications. Nanoscale Horiz 6(3):260–270. https://doi.org/10.1039/d0nh00594k
92. Yang L, Yi N, Zhu J et al (2020) Novel gas sensing platform based on a stretchable laser-induced graphene pattern with self-heating capabilities. J Mater Chem A 8(14):6487–6500. https://doi.org/10.1039/c9ta07855j
93. Yang L, Zheng GH, Cao YQ et al (2022) Moisture-resistant, stretchable NO_x gas sensors based on laser-induced graphene for environmental monitoring and breath analysis. Microsyst Nanoeng 8(1):78. https://doi.org/10.1038/s41378-022-00414-x
94. Lu YY, Fujita Y, Honda S et al (2021) Wireless and flexible skin moisture and temperature sensor sheets toward the study of thermoregulator center. Adv Healthc Mater 10(17):e2100103. https://doi.org/10.1002/adhm.202100103
95. Meng LY, Turner APF, Mak WC (2021) Conducting polymer-reinforced laser-irradiated graphene as a heterostructured 3D transducer for flexible skin patch biosensors. ACS Appl Mater Interfaces 13(45):54456–54465. https://doi.org/10.1021/acsami.1c13164
96. Liao JJ, Zhang XY, Sun ZH et al (2022) Laser-induced graphene-based wearable epidermal ion-selective sensors for noninvasive multiplexed sweat analysis. Biosensors 12(6):397. https://doi.org/10.3390/bios12060397
97. Zhang Y, Li N, Xiang YJ et al (2020) A flexible non-enzymatic glucose sensor based on copper nanoparticles anchored on laser-induced graphene. Carbon 156:506–513. https://doi.org/10.1016/j.carbon.2019.10.006

98. Yoon H, Nah J, Kim H et al (2020) A chemically modified laser-induced porous graphene based flexible and ultrasensitive electrochemical biosensor for sweat glucose detection. Sens Actuat B Chem 311:127866. https://doi.org/10.1016/j.snb.2020.127866
99. Zhu J, Liu SB, Hu ZH et al (2021) Laser-induced graphene non-enzymatic glucose sensors for on-body measurements. Biosens Bioelectron 193:113606. https://doi.org/10.1016/j.bios.2021.113606
100. Vivaldi F, Dallinger A, Poma N et al (2022) Sweat analysis with a wearable sensing platform based on laser-induced graphene. APL Bioeng 6(3):036104. https://doi.org/10.1063/5.0093301
101. Chen HQ, Mei ZF, Qi KL et al (2022) A wearable enzyme-free glucose sensor based on nickel nanoparticles decorated laser-induced graphene. J Electroanal Chem 920:116585. https://doi.org/10.1016/j.jelechem.2022.116585
102. Chen SW, Cao ZK, Zhou K et al (2023) Screen printing and laser-induced flexible sensors for the simultaneous sensitive detection of uric acid, tyrosine, and ascorbic acid in sweat. Analyst 148(13):2965–2974. https://doi.org/10.1039/d3an00591g
103. Lu YY, Xu KC, Zhang LS et al (2020) Multimodal plant healthcare flexible sensor system. ACS Nano 14(9):10966–10975. https://doi.org/10.1021/acsnano.0c03757
104. Peng B, Wu XY, Zhang C et al (2019) A flexible and fully integrated wearable pressure sensing chip system for multi-scenario applications. J Mater Chem A 9(47):26875–26884. https://doi.org/10.1039/d1ta08584k
105. Li CC, Chen HM, Zhang SC et al (2022) Wearable and biocompatible blood oxygen sensor based on heterogeneously integrated lasers on a laser-induced graphene electrode. ACS Appl Electron Mater 4(4):1583–1591. https://doi.org/10.1021/acsaelm.1c01269
106. Garland NT, Schmieder J, Johnson ZT et al (2023) Wearable flexible perspiration biosensors using laser-induced graphene and polymeric tape microfluidics. ACS Appl Mater Interfaces 15(32):38201–38213. https://doi.org/10.1021/acsami.3c04665
107. Xu KC, Li QA, Lu YY et al (2023) Laser direct writing of flexible thermal flow sensors. Nano Lett 23(22):10317–10325. https://doi.org/10.1021/acs.nanolett.3c02891
108. Lu YY, Kong DP, Yang G et al (2023) Machine learning-enabled tactile sensor design for dynamic touch decoding. Adv Sci 10(32):e2303949. https://doi.org/10.1002/advs.202303949
109. Kim D, Bang J, Won P et al (2020) Biocompatible cost-effective electrophysiological monitoring with oxidation-free Cu–Au core–shell nanowire. Adv Mater Technol 5(12):2000661. https://doi.org/10.1002/admt.202000661
110. Kedambaimoole V, Kumar N, Shirhatti V et al (2020) Laser-induced direct patterning of free-standing Ti_3C_2-MXene films for skin conformal tattoo sensors. ACS Sens 5(7):2086–2095. https://doi.org/10.1021/acssensors.0c00647
111. Chen KY, Gao C, Lu B et al (2022) A facile laser assisted paste-tear approach to large area, flexible and wearable in-plane micro-supercapacitors. J Power Sour 532:231346. https://doi.org/10.1016/j.jpowsour.2022.231346
112. Jiang XN, Zhao XP, Sun YX et al (2023) Laser-patterned PEDOT:PSS-aramid nanofiber composite electrodes for in-plane supercapacitors with high performance, shape-diversity and ultra-high deformation resistance. Chem Eng J 462:142209. https://doi.org/10.1016/j.cej.2023.142209
113. Huang KY, Ning HM, Hu N et al (2020) Ultrasensitive MWCNT/PDMS composite strain sensor fabricated by laser ablation process. Compos Sci Technol 192:108105. https://doi.org/10.1016/j.compscitech.2020.108105
114. Du XY, Shi JJ, Chen ZC et al (2020) A laser etched zinc ion microbattery with excellent flexibility and self-healability. Sustain Energy Fuels 4(9):4713–4721. https://doi.org/10.1039/d0se00843e
115. Ye XH, Qi M, Yang YF et al (2020) Pattern directive sensing selectivity of graphene for wearable multifunctional sensors via femtosecond laser fabrication. Adv Mater Technol 5(11):2000466. https://doi.org/10.1002/admt.202000446
116. Liu XM, Ueki T, Gao HY et al (2022) Microbial biofilms for electricity generation from water evaporation and power to wearables. Nat Commun 13(1):4369. https://doi.org/10.1038/s41467-022-32105-6
117. Yu YD, Zhu W, Wang YL et al (2020) Towards high integration and power density: zigzag-type thin-film thermoelectric generator assisted by rapid pulse laser patterning technique. Appl Energy 275:115404. https://doi.org/10.1016/j.apenergy.2020.115404
118. Lu YG, Ru S, Li H et al (2023) Laser-structured microarray electrodes for durable stretchable lithium-ion battery. J Colloid Interface Sci 631(Pt B):1–7. https://doi.org/10.1016/j.jcis.2022.11.024
119. Zhang S, Fei WJ, Jiang Q et al (2021) Facile fabrication of sensitivity-tunable strain sensors based on laser-patterned micro-nano structures. J Micromech Microeng 31(8):85003. https://doi.org/10.1088/1361-6439/ac0b32
120. Cho H, Jo S, Kim I et al (2021) Film-sponge-coupled triboelectric nanogenerator with enhanced contact area based on direct ultraviolet laser ablation. ACS Appl Mater Interfaces 13(40):48281–48291. https://doi.org/10.1021/acsami.1c14572
121. Liu W, Zhu CL, Wu DW et al (2020) Flexible piezoelectric micro ultrasonic transducer based on a laser processed substrate. In: IEEE International Ultrasonics Symposium, p.1–4. https://doi.org/10.1109/IUS46767.2020.9251364
122. Du QF, Liu LL, Tang RT et al (2021) High-performance flexible pressure sensor based on controllable hierarchical microstructures by laser scribing for wearable electronics. Adv Mater Technol 6(9):2100122. https://doi.org/10.1002/admt.202100122
123. Carr AR, Patel YH, Neff CR et al (2020) Sweat monitoring beneath garments using passive, wireless resonant sensors interfaced with laser-ablated microfluidics. npj Digit Med 3(1):62. https://doi.org/10.1038/s41746-020-0270-2
124. Xu ZY, Song JY, Liu BR et al (2021) A conducting polymer PEDOT:PSS hydrogel based wearable sensor for accurate uric acid detection in human sweat. Sens Actuat B Chem 348:130674. https://doi.org/10.1016/j.snb.2021.130674
125. Wolfe DB, Ashcom JB, Hwang JC et al (2003) Customization of poly(dimethylsiloxane) stamps by micromachining using a femtosecond-pulsed laser. Adv Mater 15(1):62–65. https://doi.org/10.1002/adma.200390012
126. Shin J, Ko J, Jeong S et al (2021) Monolithic digital patterning of polydimethylsiloxane with successive laser pyrolysis. Nat Mater 20(1):100–107. https://doi.org/10.1038/s41563-020-0769-6
127. Lim J, Park S, Cho H et al (2022) Monolithic digital patterning of polyimide by laser-induced pyrolytic jetting. Chem Eng J 428:131050. https://doi.org/10.1016/j.cej.2021.131050
128. Kim C, Hwang E, Kwon J et al (2023) Plastic shavings by laser: peeling porous graphene springs for multifunctional all-carbon applications. Adv Sci 10(21):e2301208. https://doi.org/10.1002/advs.202301208
129. Lee J, Sul H, Lee W et al (2020) Stretchable skin-like cooling/heating device for reconstruction of artificial thermal sensation in virtual reality. Adv Funct Mater 30(29):1909171. https://doi.org/10.1002/adfm.201909171
130. Lee J, Sul H, Jung Y et al (2020) Thermally controlled, active imperceptible artificial skin in visible-to-infrared range. Adv Funct Mater 30(36):2203328. https://doi.org/10.1002/adfm.202003328
131. Wang YL, Zhu W, Deng Y et al (2020) Self-powered wearable pressure sensing system for continuous healthcare monitoring enabled by flexible thin-film thermoelectric generator.

Nano Energy 73:104773. https://doi.org/10.1016/j.nanoen.2020.104773
132. Escobedo P, de Pablos-Florido J, Carvajal MA et al (2020) The effect of bending on laser-cut electro-textile inductors and capacitors attached on denim as wearable structures. Text Res J 90(21–22):2355–2366. https://doi.org/10.1177/0040517520920570
133. Jeong H, Feng JR, Kim J (2022) 2.5D laser-cutting-based customized fabrication of long-term wearable textile sEMG sensor: from design to intention recognition. IEEE Robot Autom Lett 7(4):10367–10374. https://doi.org/10.1109/lra.2022.3190620
134. Lipovka A, Fatkullin M, Shchadenko S et al (2023) Textile electronics with laser-induced graphene/polymer hybrid fibers. ACS Appl Mater Interfaces 15(32):38946–38955. https://doi.org/10.1021/acsami.3c06968
135. Yang GY, Ding YH, Liu L et al (2023) Mechanism and technology of laser selective removal of multilayer materials. J Mater Process Technol 312:117868. https://doi.org/10.1016/j.jmatprotec.2023.117868
136. Ding JM, Zou S, Choi J et al (2020) A laser texturing study on multi-crystalline silicon solar cells. Solar Energy Mater Solar Cell 214:110587. https://doi.org/10.1016/j.solmat.2020.110587
137. Abbott M, Cotter J (2006) Optical and electrical properties of laser texturing for high-efficiency solar cells. Prog Photovoltaics Res Appl 14(3):225–235. https://doi.org/10.1002/pip.667
138. Bondarev A, Simonovic K, Vitu T et al (2023) Textured coating or coated texture: femtosecond laser texturing of a-C:H/WC coatings for dry friction applications. Surf Coat Technol 469:129808. https://doi.org/10.1016/j.surfcoat.2023.129808
139. Shivakoti I, Kibria G, Cep R et al (2021) Laser surface texturing for biomedical applications: a review. Coatings 11(2):124. https://doi.org/10.3390/coatings11020124
140. Hwang E, Lee Y, Lim J et al (2021) Selective laser pyrolytic micropatterning of stretched elastomeric polymer surfaces. Int J Precis Eng Manuf Green Technol 8(3):795–804. https://doi.org/10.1007/s40684-020-00292-6
141. Zhang JZ, Yong JL, Zhang CJ et al (2020) Liquid metal-based reconfigurable and repairable electronics designed by a femtosecond laser. ACS Appl Electron Mater 2(8):2685–2691. https://doi.org/10.1021/acsaelm.0c00591
142. Zhang JZ, Zhang KY, Yong JL et al (2020) Femtosecond laser preparing patternable liquid-metal-repellent surface for flexible electronics. J Colloid Interface Sci 578:146–154. https://doi.org/10.1016/j.jcis.2020.05.055
143. Zhang CJ, Li ZK, Li HY et al (2022) Femtosecond laser-induced supermetalphobicity for design and fabrication of flexible tactile electronic skin sensor. ACS Appl Mater Interfaces 14(33):38328–38338. https://doi.org/10.1021/acsami.2c08835
144. Liang ST, Chen XY, Li FJ et al (2022) Laser-engraved liquid metal circuit for wearable electronics. Bioengineering 9(2):59. https://doi.org/10.3390/bioengineering9020059
145. Xu KC, Fujita Y, Lu YY et al (2021) A wearable body condition sensor system with wireless feedback alarm functions. Adv Mater 33(18):e2008701. https://doi.org/10.1002/adma.202008701
146. Koh EH, Lee WC, Choi YJ et al (2021) A wearable surface-enhanced Raman scattering sensor for label-free molecular detection. ACS Appl Mater Interfaces 13(2):3024–3032. https://doi.org/10.1021/acsami.0c18892
147. Yu J, Yang H, Wu JG et al (2023) Ultrafast laser fabrication of surface-enhanced Raman scattering sensors. Opto-Electron Eng 50(3):220333. https://doi.org/10.12086/oee.2023.220333
148. Yang H, Gun XY, Pang GH et al (2021) Femtosecond laser patterned superhydrophobic/hydrophobic SERS sensors for rapid positioning ultratrace detection. Opt Express 29(11):16904–16913. https://doi.org/10.1364/OE.423789
149. Yu J, Wu JG, Yang H et al (2022) Extremely sensitive SERS sensors based on a femtosecond laser-fabricated superhydrophobic/-philic microporous platform. ACS Appl Mater Interfaces 14(38):43877–43885. https://doi.org/10.1021/acsami.2c10381
150. Fatkullin M, Rodriguez RD, Petrov I et al (2023) Molecular plasmonic silver forests for the photocatalytic-driven sensing platforms. Nanomaterials 13(5):923. https://doi.org/10.3390/nano13050923
151. Zhou WP, Yu YC, Bai S et al (2021) Laser direct writing of waterproof sensors inside flexible substrates for wearable electronics. Opt Laser Technol 135:106694. https://doi.org/10.1016/j.optlastec.2020.106694
152. Pitkanen O, Eraslan T, Sebok D et al (2020) Flexible planar supercapacitors by straightforward filtration and laser processing steps. Nanotechnology 31(49):495403. https://doi.org/10.1088/1361-6528/abb336
153. Nguyen PT, Jang J, Lee Y et al (2021) Laser-assisted fabrication of flexible monofilament fiber supercapacitors. J Mater Chem A 9(8):4841–4850. https://doi.org/10.1039/d0ta10283k
154. Lim J, Kim Y, Shin J et al (2020) Continuous-wave laser-induced transfer of metal nanoparticles to arbitrary polymer substrates. Nanomaterials 10(4):701. https://doi.org/10.3390/nano10040701
155. Kim KK, Ha I, Kim M et al (2020) A deep-learned skin sensor decoding the epicentral human motions. Nat Commun 11(1):2149. https://doi.org/10.1038/s41467-020-16040-y
156. Kim KK, Choi J, Kim JH et al (2021) Evolvable skin electronics by in situ and in operando adaptation. Adv Funct Mater 32(4):2106329. https://doi.org/10.1002/adfm.202106329
157. Shin J, Jeong B, Kim J et al (2020) Sensitive wearable temperature sensor with seamless monolithic integration. Adv Mater 32(2):e1905527. https://doi.org/10.1002/adma.201905527
158. Cui SY, Lu YY, Kong DP et al (2023) Laser direct writing of Ga_2O_3/liquid metal-based flexible humidity sensors. Opto-Electron Adv 6(7):220172. https://doi.org/10.29026/oea.2023.220172
159. Kim M, Cho C, Shin W et al (2022) Nanowire-assisted freestanding liquid metal thin-film patterns for highly stretchable electrodes on 3D surfaces. npj Flex Electron 6(1):99. https://doi.org/10.1038/s41528-022-00232-1
160. Kim M, Park JJ, Cho C et al (2023) Liquid metal based stretchable room temperature soldering sticker patch for stretchable electronics integration. Adv Funct Mater 33(36):2303286. https://doi.org/10.1002/adfm.202303286
161. Kim H, Choi J, Kim KK et al (2021) Biomimetic chameleon soft robot with artificial crypsis and disruptive coloration skin. Nat Commun 12(1):4658. https://doi.org/10.1038/s41467-021-24916-w
162. Yeo J, Hong S, Kim G et al (2015) Laser-induced hydrothermal growth of heterogeneous metal-oxide nanowire on flexible substrate by laser absorption layer design. ACS Nano 9(6):6059–6068. https://doi.org/10.1021/acsnano.5b01125
163. Mun J, Kong H, Lee J et al (2023) Enhanced photocurrent performance of flexible micro-photodetector based on PN nanowires heterojunction using all-laser direct patterning. Adv Funct Mater 33(24):2214950. https://doi.org/10.1002/adfm.202214950
164. Liang SY, Dai YZ, Wang G et al (2020) Room-temperature fabrication of SiC microwire photodetectors on rigid and flexible substrates via femtosecond laser direct writing. Nanoscale 12(45):23200–23205. https://doi.org/10.1039/d0nr05299j
165. Dai YZ, Liang SY, Lv C et al (2020) Controllably fabricated single microwires from Pd-WO_3•xH_2O nanoparticles by femtosecond laser for faster response ammonia sensors at room temperature. Sens Actuat B Chem 316:128122. https://doi.org/10.1016/j.snb.2020.128122
166. Chang PY, Lin CF, El Khoury RS et al (2020) Near-infrared laser-annealed IZO flexible device as a sensitive H_2S sensor at room

temperature. ACS Appl Mater Interfaces 12(22):24984–24991. https://doi.org/10.1021/acsami.0c03257
167. Gao L, Wang XH, Dai WT et al (2020) Laser direct writing assisted fabrication of skin compatible metal electrodes. Adv Mater Technol 5(5):2000012. https://doi.org/10.1002/admt.202000012
168. Zhang YL, Lu HL, Li M et al (2021) Near-infrared laser "weldable" hydrogen-bonded hydrogel sensor based on photothermal gel–sol transition. ACS Sustain Chem Eng 9(48):16241–16250. https://doi.org/10.1021/acssuschemeng.1c05510
169. Fromme NP, Li YF, Camenzind M et al (2021) Metal-textile laser welding for wearable sensors applications. Adv Electron Mater 7(4):2001238. https://doi.org/10.1002/aelm.202001238
170. Hwang Y, Park B, Hwang S et al (2023) A bioinspired ultra flexible artificial van der Waals 2D-MoS_2 channel/$LiSiO_x$ solid electrolyte synapse arrays via laser-lift off process for wearable adaptive neuromorphic computing. Small Methods 7(7):e2201719. https://doi.org/10.1002/smtd.202201719
171. Lee J, Jung Y, Lee M et al (2022) Biomimetic reconstruction of butterfly wing scale nanostructures for radiative cooling and structural coloration. Nanoscale Horiz 7(9):1054–1064. https://doi.org/10.1039/d2nh00166g
172. Zhang J, Zhang T, Zhang H et al (2020) Single-crystal SnSe thermoelectric fibers via laser-induced directional crystallization: from 1D fibers to multidimensional fabrics. Adv Mater 32(36):e2002702. https://doi.org/10.1002/adma.202002702
173. Lim J, Goh B, Qu WH et al (2022) Adhesive-free bonding of PI/PDMS interface by site-selective photothermal reactions. Appl Surf Sci 571:151123. https://doi.org/10.1016/j.apsusc.2021.151123
174. Won D, Kim J, Choi J et al (2022) Digital selective transformation and patterning of highly conductive hydrogel bioelectronics by laser-induced phase separation. Sci Adv 8(23):eabo3209. https://doi.org/10.1126/sciadv.abo3209
175. Kong H, Kwon J, Paeng D et al (2020) Laser-induced crystalline-phase transformation for hematite nanorod photoelectrochemical cells. ACS Appl Mater Interfaces 12(43):48917–48927. https://doi.org/10.1021/acsami.0c11999
176. Bang J, Jung Y, Kim H et al (2022) Multi-bandgap monolithic metal nanowire percolation network sensor integration by reversible selective laser-induced redox. Nanomicro Lett 14(1):49. https://doi.org/10.1007/s40820-021-00786-1
177. Yang YR, Song Y, Bo XJ et al (2020) A laser-engraved wearable sensor for sensitive detection of uric acid and tyrosine in sweat. Nat Biotechnol 38(2):217–224. https://doi.org/10.1038/s41587-019-0321-x
178. Nah JS, Barman SC, Zahed MA et al (2021) A wearable microfluidics-integrated impedimetric immunosensor based on Ti_3C_2T MXene incorporated laser-burned graphene for noninvasive sweat cortisol detection. Sens Actuat B Chem 329:129206. https://doi.org/10.1016/j.snb.2020.129206
179. Yan WH, Yan WR, Chen TD et al (2020) Size-tunable flowerlike MoS_2 nanospheres combined with laser-induced graphene electrodes for NO_2 sensing. ACS Appl Nano Mater 3(3):2545–2553. https://doi.org/10.1021/acsanm.9b02614
180. Wang G, Zhang Y, Yang H et al (2020) Fast-response humidity sensor based on laser printing for respiration monitoring. RSC Adv 10(15):8910–8916. https://doi.org/10.1039/c9ra10409g
181. Nam VB, Shin J, Choi A et al (2021) High-temperature, thin, flexible and transparent Ni-based heaters patterned by laser-induced reductive sintering on colorless polyimide. J Mater Chem C 9(17):5652–5661. https://doi.org/10.1039/d1tc00435b
182. Zhang P, Tang XL, Pang Y et al (2020) Flexible laser-induced-graphene omnidirectional sound device. Chem Phys Lett 745:137275. https://doi.org/10.1016/j.cplett.2020.137275
183. Luo HY, Lu YY, Xu YH et al (2022) A fully soft, self-powered vibration sensor by laser direct writing. Nano Energy 103:107803. https://doi.org/10.1016/j.nanoen.2022.107803
184. Song Y, Min JH, Yu Y et al (2020) Wireless battery-free wearable sweat sensor powered by human motion. Sci Adv 6(40):eaay9842. https://doi.org/10.1126/sciadv.aay9842
185. Velmurugan R, Alagammai P, Ulaganathan M et al (2020) High performance in situ annealed partially pressurized pulsed laser deposited WO_3 & V_2O_5 thin film electrodes for use as flexible all solid state supercapbatteries. J Mater Chem A 8(45):24148–24165. https://doi.org/10.1039/d0ta07683j
186. Capuron L, Schroecksnadel S, Feart C et al (2011) Chronic low-grade inflammation in elderly persons is associated with altered tryptophan and tyrosine metabolism: role in neuropsychiatric symptoms. Biol Psychiatry 70(2):175–182. https://doi.org/10.1016/j.biopsych.2010.12.006
187. Major TJ, Dalbeth N, Stahl EA et al (2018) An update on the genetics of hyperuricaemia and gout. Nat Rev Rheumatol 14(6):341–353. https://doi.org/10.1038/s41584-018-0004-x
188. Nayak P, Kurra N, Xia C et al (2016) Highly efficient laser scribed graphene electrodes for on-chip electrochemical sensing applications. Adv Electron Mater 2(10):1600185. https://doi.org/10.1002/aelm.201600185
189. Griffiths K, Dale C, Hedley J et al (2014) Laser-scribed graphene presents an opportunity to print a new generation of disposable electrochemical sensors. Nanoscale 6(22):13613–13622. https://doi.org/10.1039/c4nr04221b
190. Lu YY, Yang G, Wang SQ et al (2023) Stretchable graphene–hydrogel interfaces for wearable and implantable bioelectronics. Nat Electron 7(1):51–65. https://doi.org/10.1038/s41928-023-01091-y
191. Le TSD, Phan HP, Kwon S et al (2022) Recent advances in laser-induced graphene: mechanism, fabrication, properties, and applications in flexible electronics. Adv Funct Mater 32(48):2205258. https://doi.org/10.1002/adfm.202205158
192. Noh J, Ha J, Kim D (2020) Femtosecond and nanosecond laser sintering of silver nanoparticles on a flexible substrate. Appl Surf Sci 511:145574. https://doi.org/10.1016/j.apsusc.2020.145574
193. Park M, Gu YR, Mao XL et al (2023) Mechanisms of ultrafast GHz burst fs laser ablation. Sci Adv 9(12):eadf6397. https://doi.org/10.1126/sciadv.adf6397